nature energy

Article

https://doi.org/10.1038/s41560-023-01194-y

High-throughput Li plating quantification for fast-charging battery design

In the format provided by the authors and unedited

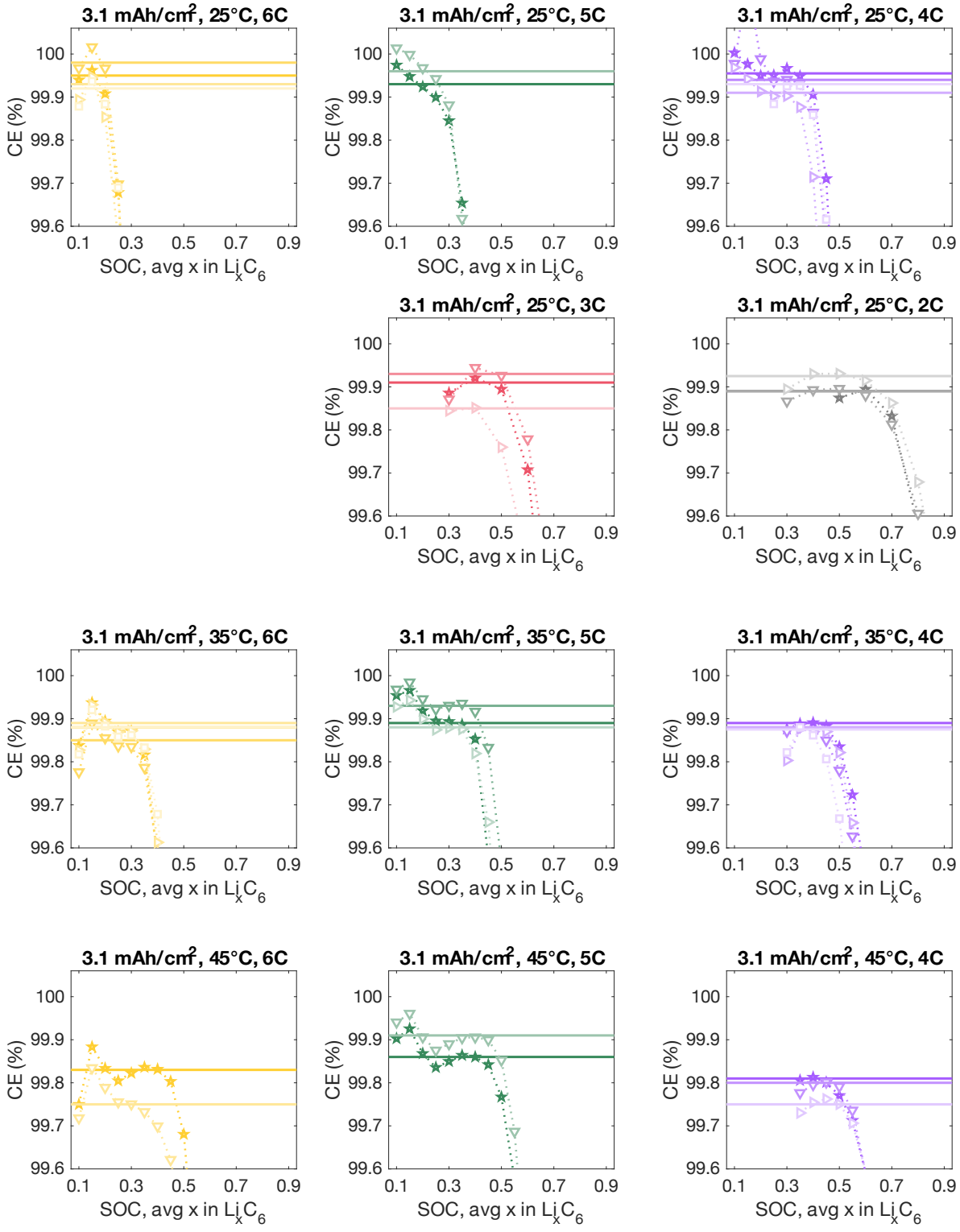

Supplementary Fig. 1 | Coulombic Efficiency Baseline Fitting for all Fig. 1,2a-f data – 3.1 mAh/cm^2

The CE baselines, shown as horizontal lines, were unique to each cell and fit manually due to some transient CE behavior sometimes observed during the first 1-3 cycles. The SOC for which CE's are collected is described in the Methods and Supplementary Table 2. The baseline is either assigned near a) the y-value of an observed CE plateau (repeated CE measurements within ~0.02% even as cycle capacity/SOC varies) or b) near the maximum

measured CE value. Sometimes the first 3 fast charging cycles (leftmost 3 datapoints in a series) exhibit increasing (Supplementary Fig. 2, middle row left column) or decreasing (Supplementary Fig. 1, top row middle column) trends with SOC. We first note that the magnitude of these drifts are very small, typically <0.02% CE per cycle, whereas the clear CE drops near the onset of plating are >0.1% CE. Second, those first cycles have the lowest intercalation capacities (SOC or mAh), which is the denominator of CE, so those CE values are most sensitive to small changes in deintercalation capacity (the numerator). Physically, we attribute the increasing CE to additional SEI formation losses on the first few cycles. The decreasing CE may occur due to slight electrode de-wetting or active material loss in coin cells due to experimental error in fabrication. However, for all these slight variations, the expected trends of lithium plating are still observed, giving us confidence in the robustness of the method, as discussed related to Figs. 1c, 2a-g in the main manuscript.

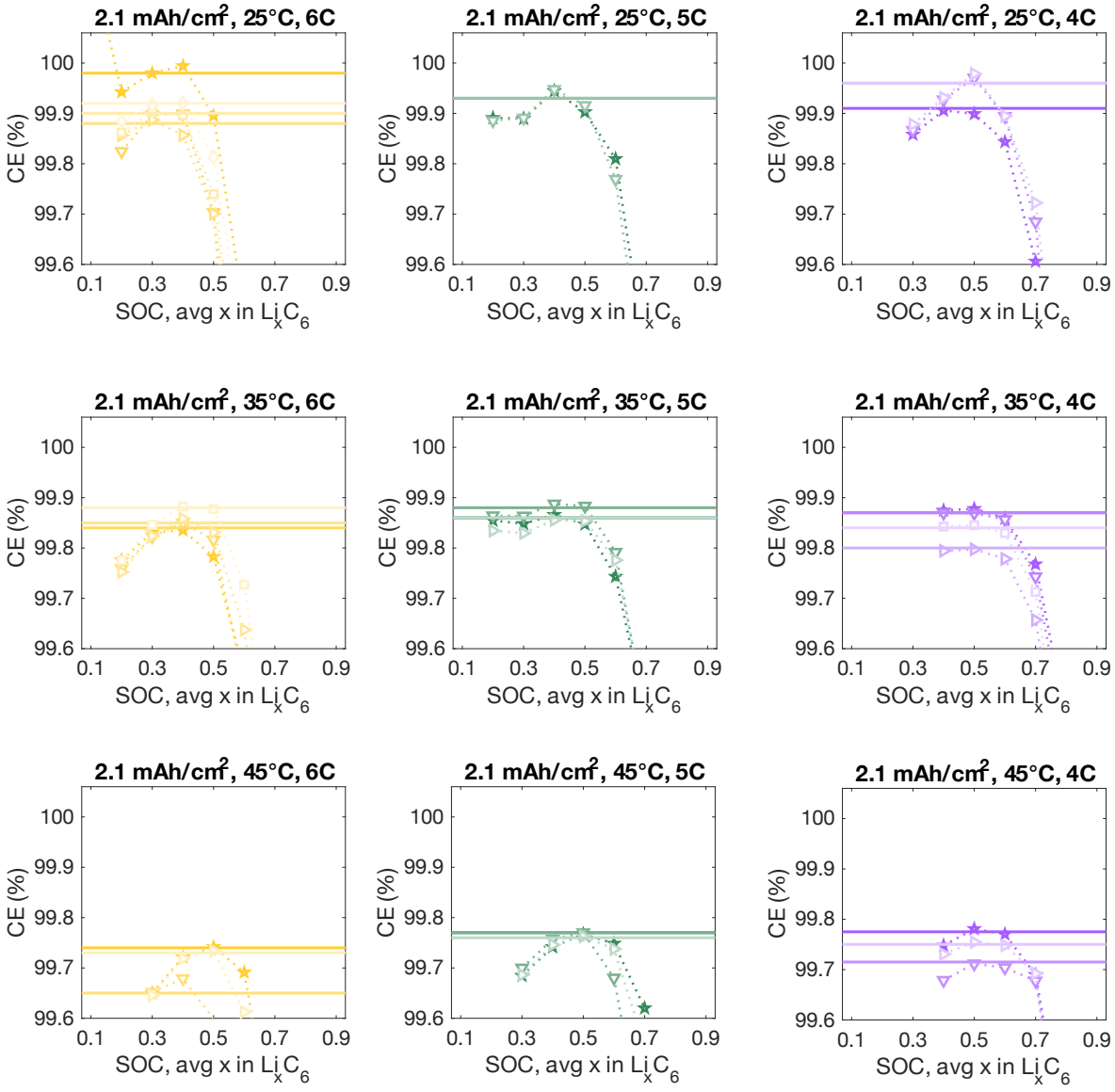

Supplementary Fig. 2 | Coulombic Efficiency Baseline Fitting for all Fig. 1,2a-f data – 2.1 mAh/cm^2
The CE baselines, shown as horizontal lines, were unique to each cell and fit manually due to some transient CE behavior sometimes observed during the first 1-3 cycles.

Supplementary Table 1 | Baseline Coulombic Efficiency Dependence on Loading and Temperature

The baseline coulombic efficiency corresponding to the absence of Li plating is visually observed to decrease with temperature in Supplementary Fig. 1, so here we quantify the dependence across all cells, grouped by loading and T. The clear temperature dependence, regardless of loading and rate, may suggest increased continual SEI dissolution during the long C/5 discharge steps that results in lost capacity to additional SEI formation on the next cycle. It is important to remember that all cells are cycled fewer than 20 times, so we expect the SEI to be fairly thin and undergo slight continued growth throughout the protocol. Especially for the first few fast charge cycles, capacity loss to additional SEI formation is expected because the rapid graphite expansion with phase change is likely to compromise some parts of SEI. High temperature is known to promote battery self-discharge, and at the graphite electrode many parasitic reactions form new SEI, so we believe this is a reasonable hypothesis. The slow C/5 deintercalation and 30 min rest between current steps means the cycles last ~3-5 hours, sufficient time for additional ~0.04% self-discharge at elevated temperature with nascent SEI.

	25℃	**35℃**	**45℃**
3.1 mAh/cm^2	99.92 ± 0.03	99.88 ± 0.02	99.82 ± 0.06
2.1 mAh/cm^2	99.93 ± 0.02	99.85 ± 0.02	99.74 ± 0.04

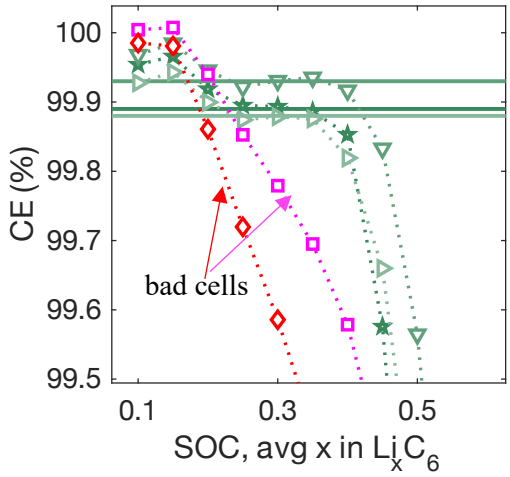

Supplementary Fig. 3 | Removing data from 'bad cells' and ensuring experiment fidelity by CE inspection

Typically 3 cells were run initially at each condition in Fig. 2a, but the number of cells reported varies between 2 and 5 (Fig. 2a-f, bottom left of each panel). An additional set of 2-3 cells may have been run for better data statistics or to make up for data that was excluded due to indicators of poor cell performance. The above figure shows 2 cells in red diamonds and pink squares, for example, at the [5C, 3.1 mAh/cm^2, 35°C] condition, that were excluded. Compared with the other data, the coulombic efficiency decreases linearly and continuously with increasing SOC, either indicating an outlier for the onset of irreversible lithium plating by 15-20% SOC or other rapid cell aging mechanisms. Given the experimental imperfections in manual cell fabrication, we attribute this behavior to bad electrode alignment which may result in early lithium plating on the conductive spacers or other cell parts instead of the graphite electrode. Observing these anomalies, however, increases the fidelity of the 'good' data used for analysis and also motivates the need for automated cell manufacturing methods to reduce human error. It is important to note that the extreme conditions of fast charging and the heterogeneous nature of lithium plating exacerbate the smallest cell defects, so some bad data should be expected, further motivating the need for adequate statistics of Li plating studies.

Supplementary Table 2 | SOC-sweep range selection for Li|Graphite plating onset experiments

These are the SOC cutoffs tested for the fast charging cycles, in order of low to high SOC (see manuscript methods) for all loadings, temperatures, and C-rates reported for Fig. 2 (white), Supplementary Fig. 13 (orange), Fig. 3a (green), and Fig. 5b (blue). The nomenclature [20:10:80] means that the first cycle charged to 20%, the last cycle charged to 80%, and the intermediate cycles were incremented by 10% SOC. **Discussion:** For conditions with anticipated Li plating onsets at high SOC, larger SOC increments were selected (10% instead of 5%) to i) reduce experiment time given slow C/5 graphite deintercalation to 1.5V and ii) limit Li metal electrode aging effects.

	25°C	30°C	35°C	45°C
Anode A1 ($2.1\ mAh/cm^2$)	6C [20:10:80] 5C [20:10:80] 4C [30:10:90]		6C [20:10:70] 5C [20:10:80] 4C [40:10:90]	6C [30:10:90] 5C [30:10:90] 4C [40:10:90]
Anode A2 ($3.1\ mAh/cm^2$)	6C [10:5:35] 5C [10:5:50] 4C [10:5:55] 4C [10:5:80] (Fig. 3a) 3C [30:10:90] 2C [30:10:90]		6C [10:5:60] 5C [10:5:60] 4C [30:5:80]	6C [10:5:70] 5C [10:5:70] 4C [30:5:80]
Anode A3 ($3.35\ mAh/cm^2$)		6C [10:5:40] 4C [10:5:55] 3C [25:5:70] (Fig. 5b)		
Anode A4 ($3.75\ mAh/cm^2$)		5.5C [10:5:40] (Fig. S11) 3.5C [10:5:60]		

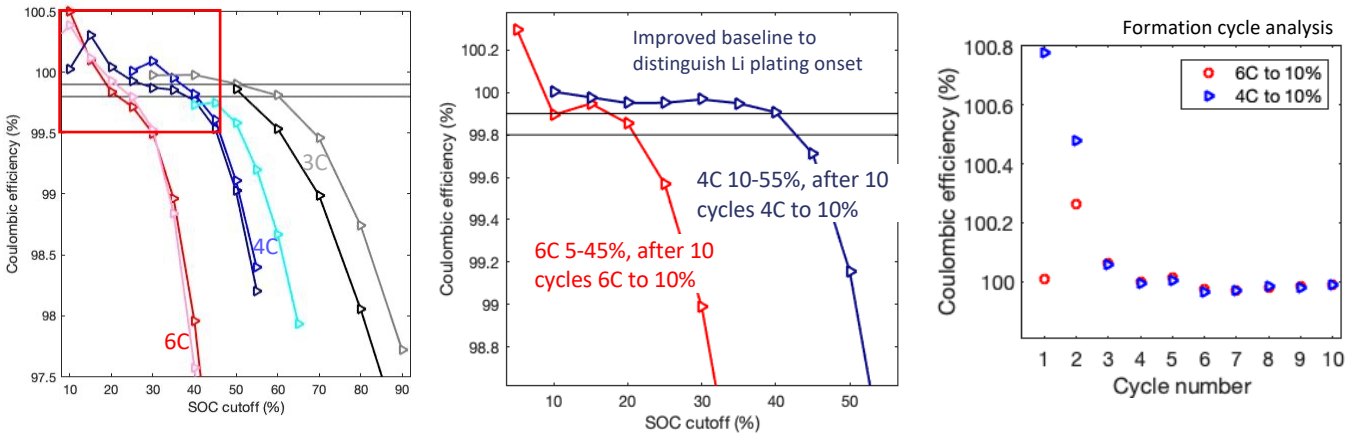

Supplementary Fig. 4 | Motivation for Li|Graphite cell Fast Formation before SOC-sweep

Left, Results from the fast charging SOC-sweep protocol for Li|Graphite cells with 3 C/10 formation cycles only shows drifting, noisy CE's that make it difficult to baseline and quantify Li plating (red box). **Center,** Fast charging SOC-sweep results after 10 cycles of 6C to 10% SOC (red) and 10 cycles of 4C to 10% SOC (blue) were added to the standard formation protocol. **Right,** The CEs for the fast-formation cycles to 10% show stabilization near Cycle 4, justifying the selection of 5 cycles of 4C intercalation to 10% as the added fast formation protocol. **Discussion:** We emphasize the importance of having stable baseline CEs prior to the Li plating onset for accurate irreversible Li quantification from the coulombic inefficiency, and note that the optimal formation protocol may differ depending on specific cell geometry. This is one reason why the SOC-sweep protocol should have multiple (>3) cycles to low SOC before the expected Li plating onset, to enable clear baseline CE fitting. This rule of thumb helped inform the SOC-sweep range selection above.

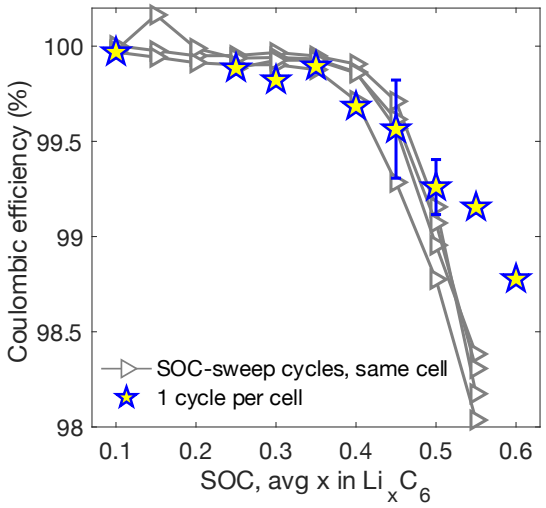

Supplementary Fig. 5 | Control experiments to understand SOC-sweep protocol cell aging effect

An initial concern with the SOC-sweep protocol was whether the early SOC cycling affected the onset and amount of irreversible Li plating, which would be an undesirable aging effect for comparing results across cells with Li plating at different conditions. Here we show that for the [4C, 3.1 mAh/cm^2, 25°C] condition, coulombic efficiencies recorded from the SOC-sweep, in which cycles were all performed on the same cell (grey, n=4 cells), match very closely with CE's taken with only 1 fast charging cycle per cell (stars, n=13 cells, replicates recorded for 0.40-0.55 SOC, standard deviation shown although too small to see for 0.4 and 0.55 SOC). Despite some expected transient behavior for the CE of the first fast charging cycle (leftmost data points in Supplementary Fig. 1 and 2 curves, at low SOC), the data show excellent agreement for the onset of CE drop and irreversible Li plating from 40-50% SOC. For cycles to higher SOC far beyond the plating onset, more loss is observed for the SOC-sweep cells that have a history of Li plating. This is expected as the accumulation of small amounts of dead Li plating can provide nucleation sites for increased Li plating on future cycles and/or disrupt Li^+ electrolyte transport through the porous electrode, leading to increased plating. However, this work performs quantitative analysis only on the plating onset region and small irreversible Li amounts, so we believe this aging effect is not a concern to the present study. In commercial cells, of course we expect cell aging and changes in cell resistances to affect Li plating onsets, but those effects become significant on the order of 10^2-10^3 cycles instead of the ~7-12 cycles performed here.

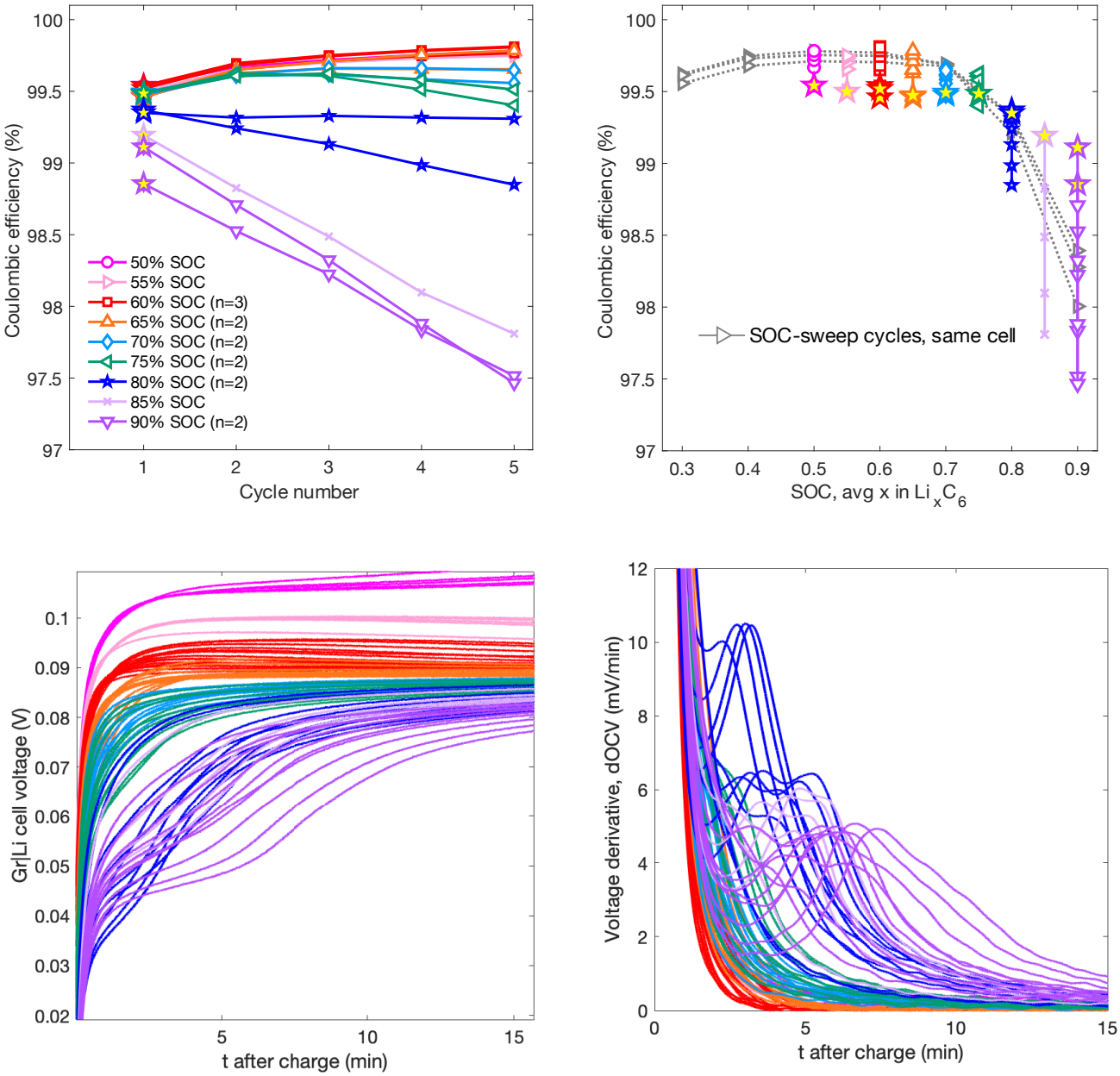

Supplementary Fig. 6 | Confirming the presence of Li plating and experiment validation at 45°C

Here we confirm that Li plating is the dominant mechanism of capacity loss at high temperatures instead of other possible cell degradation or Li metal electrode aging. For the [4C, 2.1 mAh/cm^2, 45°C] condition, we cycled cells 5 times to a single SOC, ranging 50-90% SOC, and the CEs are plotted in the top left. A star represents the efficiency for the first fast charging cycle. The first sign that cell aging related to the Li metal electrode is not causing the drop in CE is that for 50-65% SOC, the coulombic efficiency continually increases with cycling. This suggests no Li plating at these SOC and the continual formation of a more temperature-resistive SEI. Next, we compare the CEs for each cell with CE's recorded from the SOC-sweep method, data presented in Fig. 2a-f. The overlay shows excellent agreement between the single-SOC and SOC-sweep efficiencies. For Li plating conditions, it is expected that the CE decrease with cycling to that SOC due to previously discussed aging effects in Supplementary Fig. 2. The earliest SOC at which this behavior occurs is 70-75%, which agrees well with the plating onset of ~71% SOC reported for this condition using the SOC-sweep in Fig. 2g. To confirm the presence of Li plating, the voltage relaxation after charge (bottom left) and corresponding derivative (bottom right) are plotted and show the characteristic voltage plateau/derivative peak feature that signals Li^0 re-intercalation[1–3] at 80% SOC and above, consistent with the method's sensitivity for Li plating detection[4].

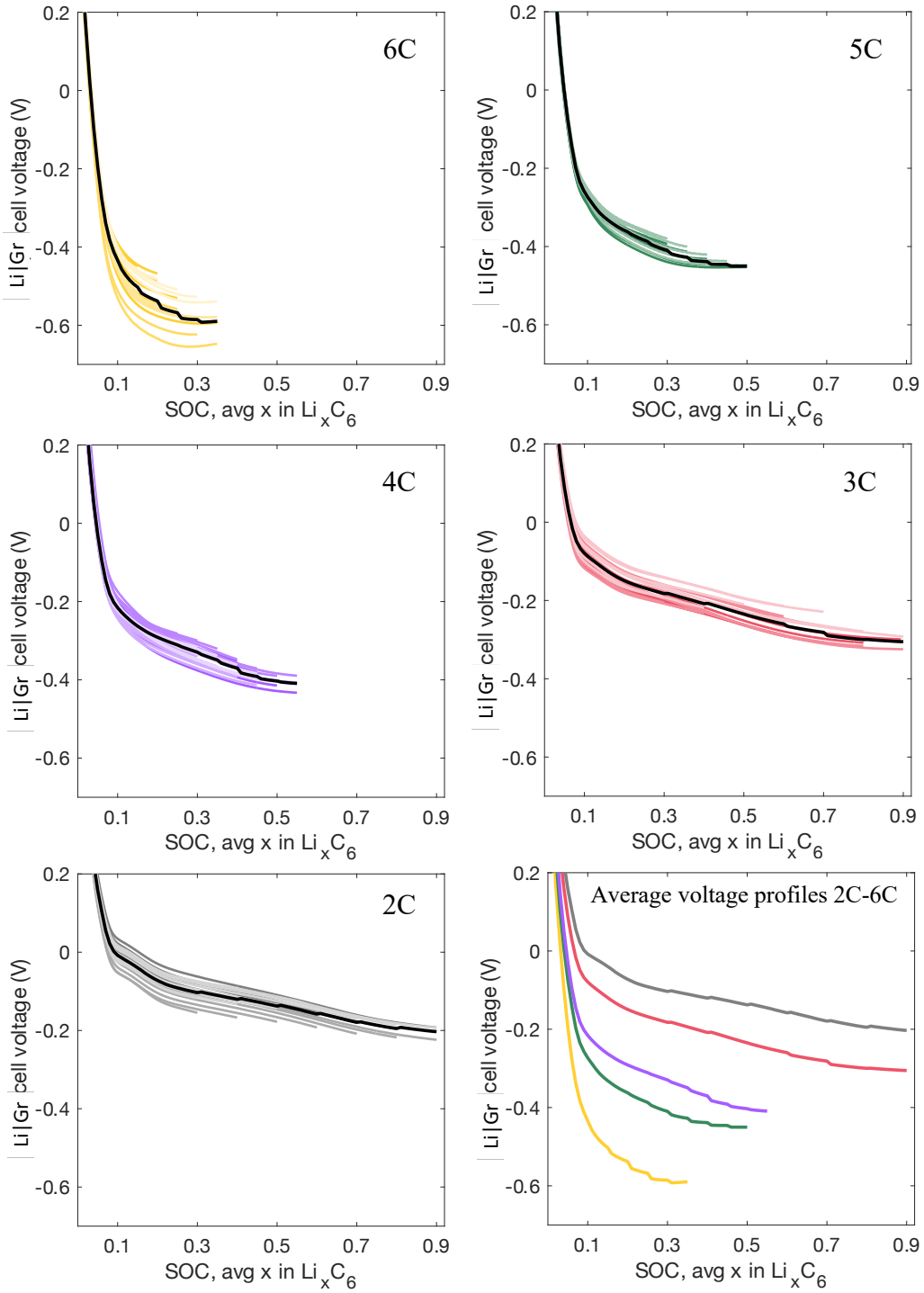

Supplementary Fig. 7 | Calculating average experimental voltage profiles for model comparison
Due to variability in cell-to-cell preparation, resistances vary slightly by sample. We calculate average experimental voltage profiles for each [rate, loading, temperature] combination across all cells and fast charging cycles. Shown here is the averaging for the 3.1 mAh/cm^2 and 25°C data from Fig. 1c/2a. The average voltage profiles are shown in the bottom right, and note that the discontinuities every 5-10% SOC are artefacts of cell resistance drifting with aging. We do not observe any correlation with cell resistances and Li plating behavior within data for a given C-rate. For example, 2 identically constructed and cycled cells may have slightly different resistances, and the one with a larger overpotential (more negative average voltage) does not necessarily show an earlier plating onset or larger amount of irreversible Li plating.

Supplementary Table 3 | Model parameters for Li|Graphite cells

C_e is the local salt concentration in mol/L and x is local graphite intercalation fraction.

Parameter	Graphite Electrode 2.1 mAh/cm^2 / 3.1 mAh/cm^2	Separator	Lithium
Thickness (μm)	47/70	25	N/A
Porosity (%)	37.4/35.4	55	N/A
Particle Radius, r_p (μm)	4	N/A	N/A
Bruggeman Exponent	2.1	2.0	N/A
Exchange current density, i_0 (A·m^{-2})	$0.3\ (C_e)^{0.5}(C_s)^{0.5}(C_s - C_s^{max})^{0.5}$	N/A	10
Activation energy for exchange current density (kJ/mol)	30	N/A	50
Solid-state Diffusion Coefficient, D_s (m^2·s^{-1})	$3E\text{-}14(1.5 - x)^{2.5}$	N/A	N/A
Activation energy for solid-state diffusion (kJ/mol)	15	N/A	N/A
Maximum Intercalated Lithium Concentration, C_s^{max} (kmol·m^{-3})	28.0	N/A	N/A

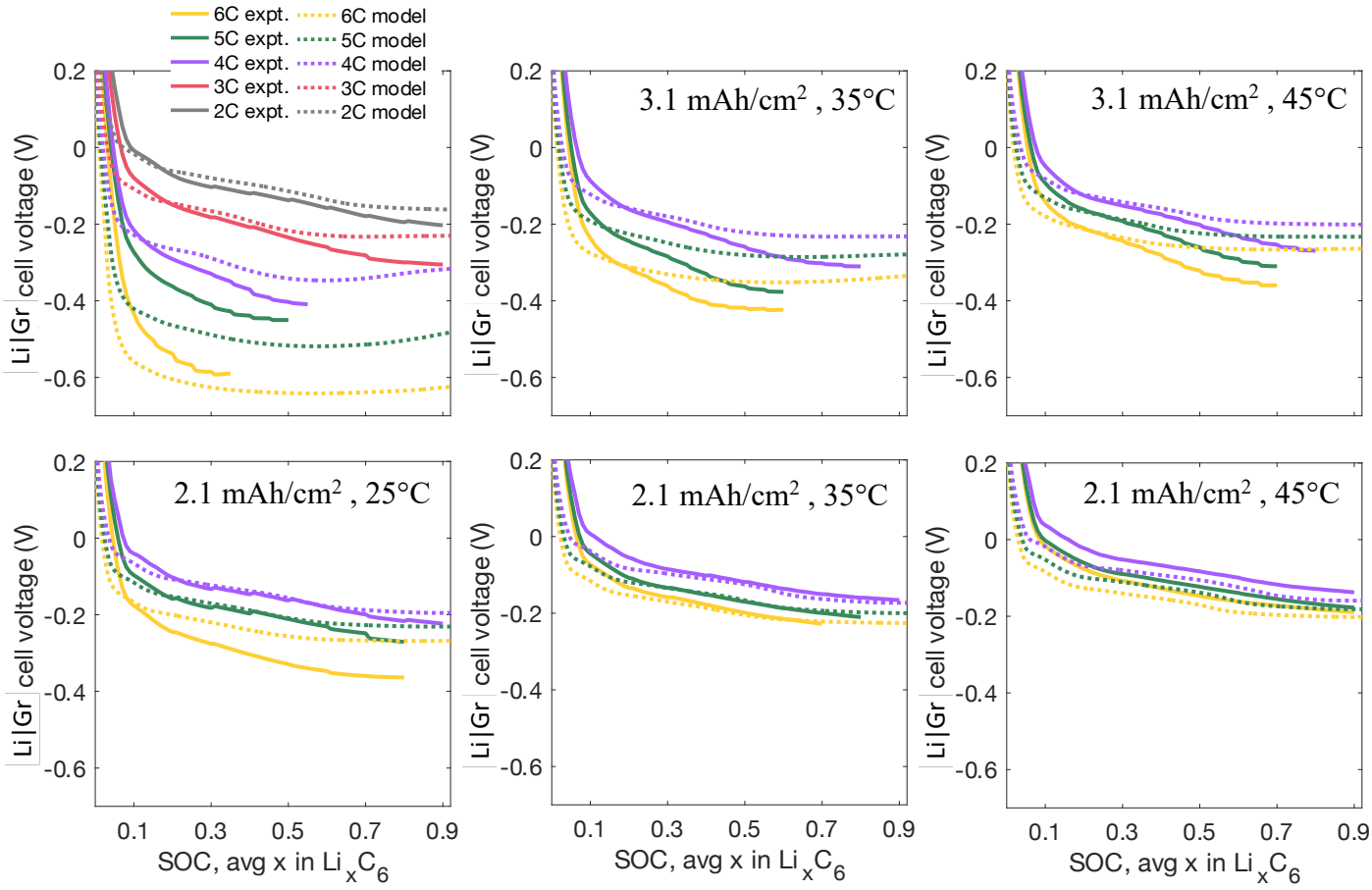

Supplementary Fig. 8 | Model-Experiment Voltage Profile Comparison

Experimental average voltage profiles in Li|Graphite cells (see Supplementary Fig. 7) show good agreement with simulated voltages from the Electrochemical Model. Discrepancies at higher SOC and temperature for the top right panels may be due to Li metal electrode resistance increase/drift with SOC-sweep cycling, seen in Supplementary Fig. 7.

Note: At high rates, many time-varying overpotentials contribute to the total cell voltage, so the 0.05 V difference that distinguishes the graphite phase plateaus would be difficult to distinguish even with uniform graphite lithiation. Models and experiment show that many lithiation phases exist simultaneously during fast charging, with higher lithiation phases such as LiC_6 being formed near the graphite|separator interface due to electrolyte ion transport limitations.

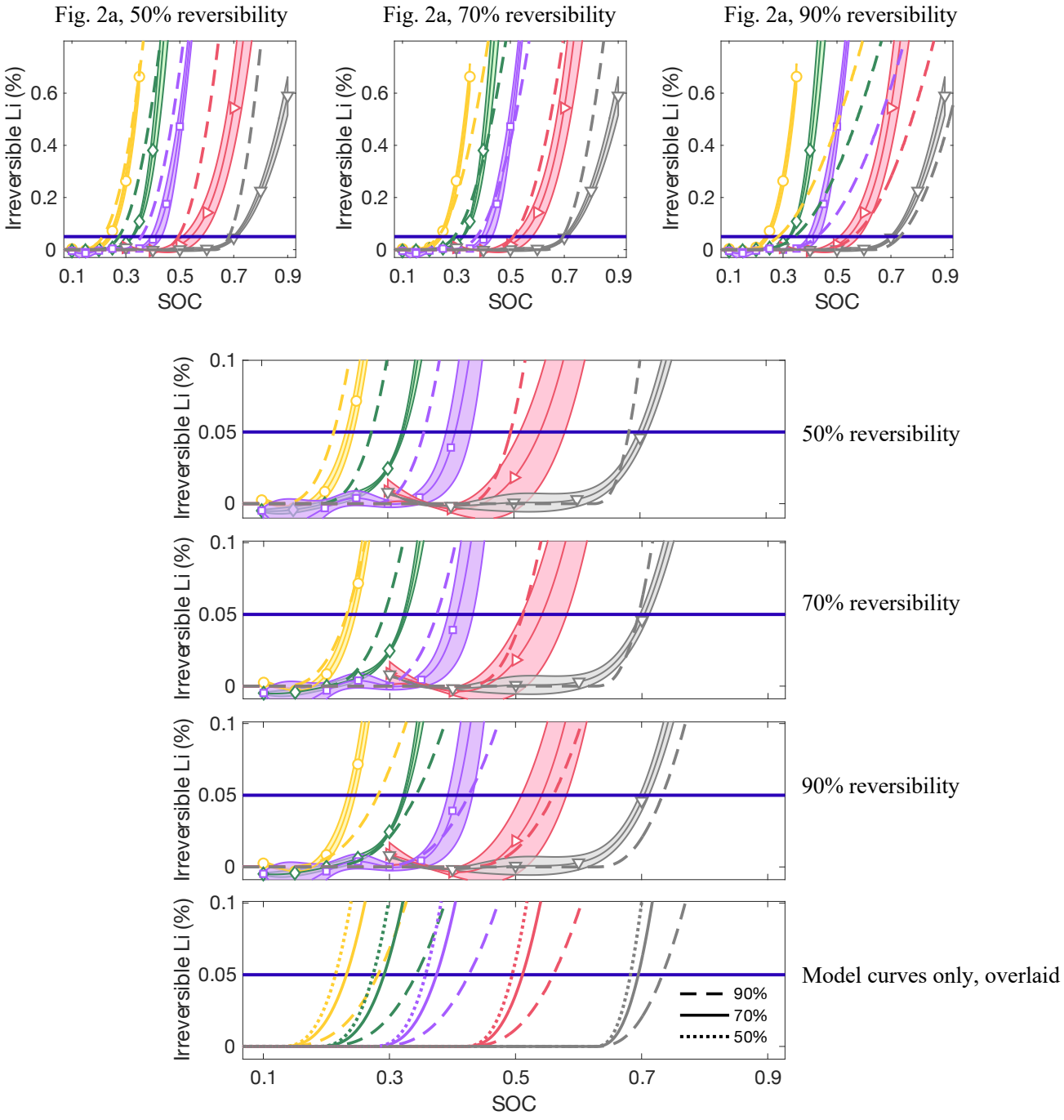

Supplementary Fig. 9 | Visualizing how varying the reversibility parameter affects simulated irreversible Li

The model outputs a quantity of total lithium plating, and a single reversibility parameter is used to scale that amount to plot the irreversible Li, as detailed in the Methods. At the top, Fig. 2a experiment data is shown for reference, and the model results are shown for varied Li plating reversibility. Increasing reversibility decreases the slope of the curve (left to right, dashed lines). The large panels below zoom in on the Li plating onset region, showing that a change in reversibility from 50-90% can change the onset of 0.05% Irreversible Li plating by up to ~7% SOC.

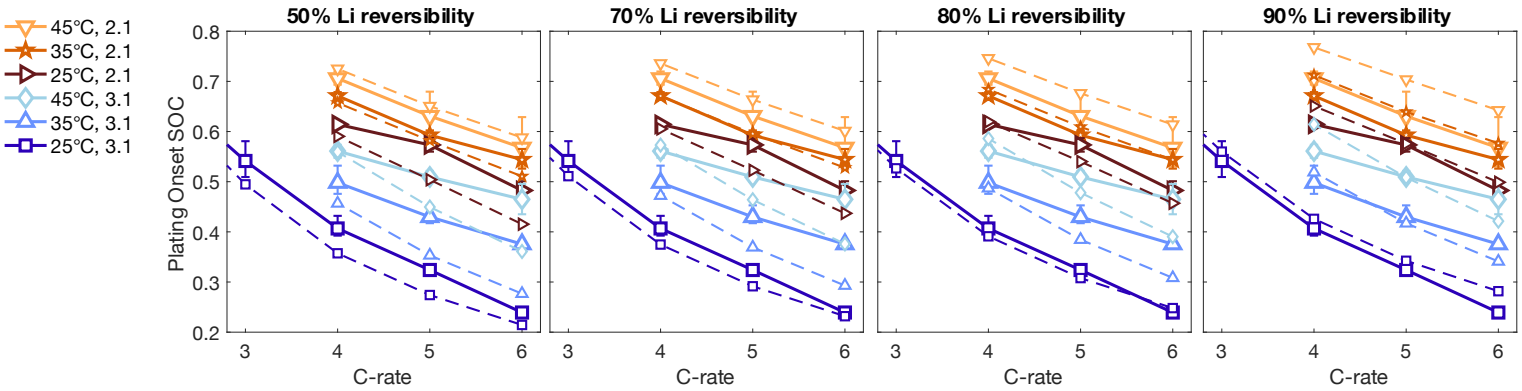

Supplementary Fig. 10 | Model-experiment plating onset comparison as model Li reversibility is varied

Computing the universal Li plating reversibility that minimizes Model-experiment error (Fig. 4f) requires first calculating new model Li plating onsets for each reversibility. Plotted above are the experimental Li plating onsets of Fig. 2g, fixed, compared with plating onsets from the model at different reversibilities. The sum of squared errors was calculated over all 20 [c, x, T] pairs, except [6, 3.1, 35] and [6, 3.1, 45], which were removed because they had nearly 10% SOC error in the initial plating onset analysis which was expected to skew the results towards high plating reversibility. Error bars are calculated in the same manner described in Fig. 2g.

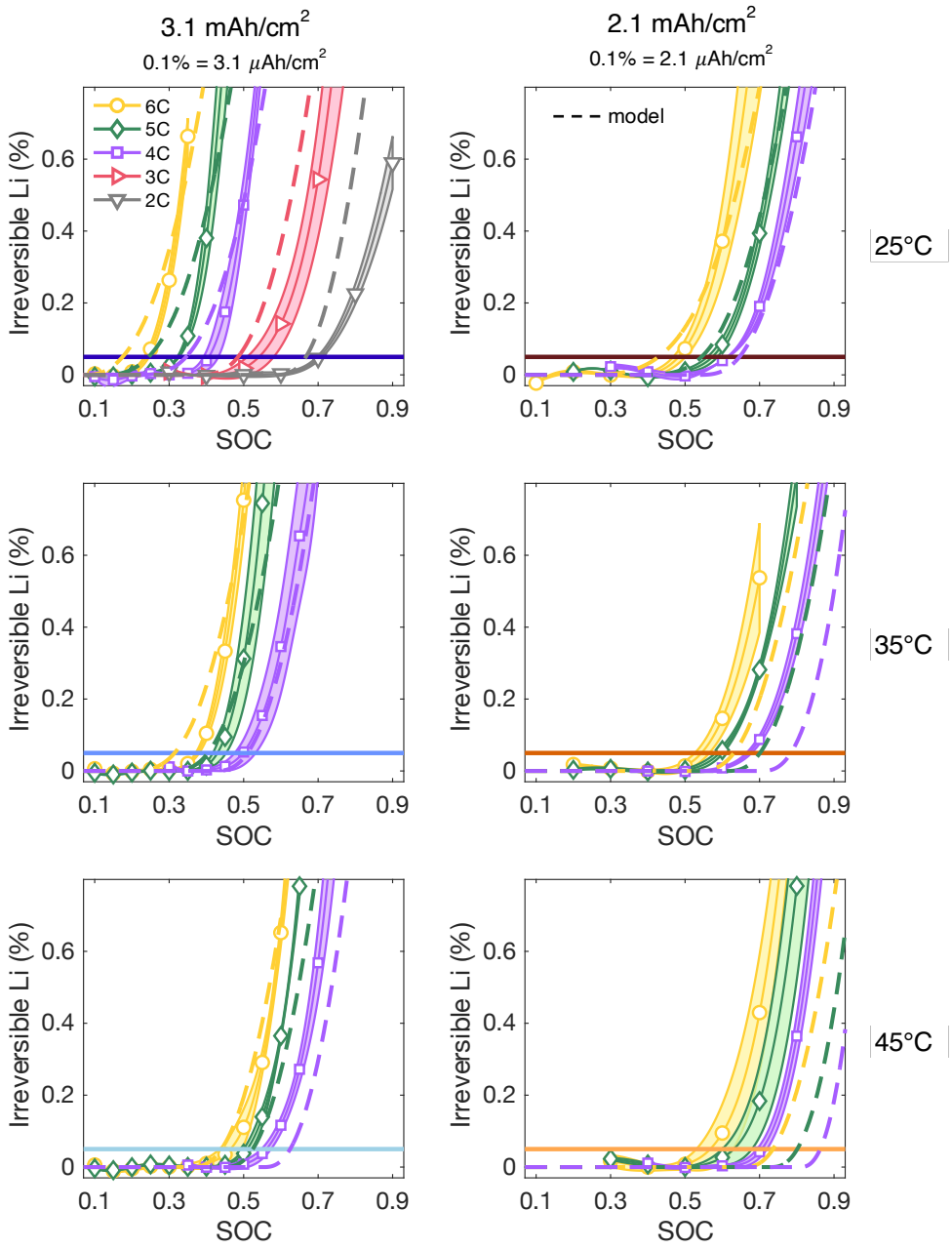

Supplementary Fig. 11 | Model-experiment comparison before changing solid-state Li diffusion parameters

The primary model change from previous works[5–7] to obtain Fig. 2a-f model outputs was incorporating intercalation fraction dependence on solid-state diffusion and decreasing the solid-state diffusion activation energy from 30 to 15 kJ/mol. Above are the experiment-model comparisons before those changes were applied. The most significant disagreement was observed at high temperatures for the low-loading electrodes.

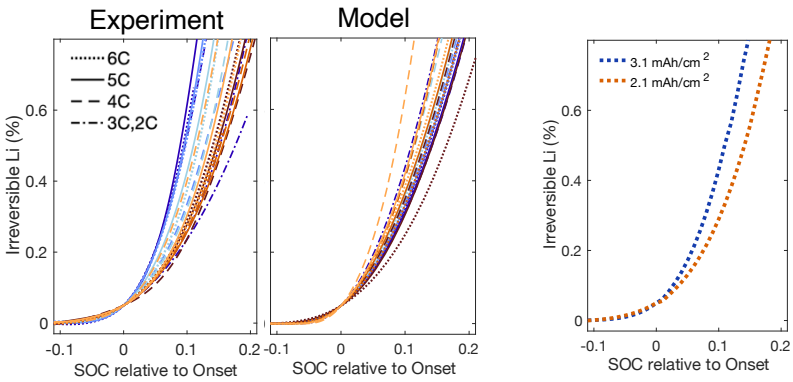

Supplementary Fig. 12 | Experimental and modeled irreversible Li plating curves overlaid

Experimental average and modeled irreversible Li plating curves from Figs. 2a-f shifted in the x-direction by their respective plating onset SOC. The colors correspond to the unique [temperature, loading] combinations as in Fig. 2a-f (also Supplementary Fig. 10 above), and the rate is depicted by the line style. The average experimental irreversible Li curve by loading is seen on the right. Irreversible Li accumulates faster (at lower SOC) for the 3.1 mAh/cm^2 electrode.

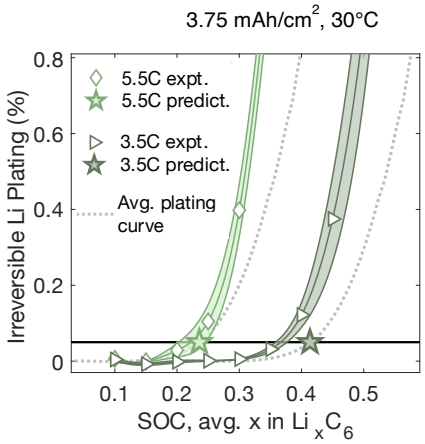

Supplementary Fig. 13 | Empirical fitting prediction accuracy graphite loading outside of experimental range

The fitting predicts the lithium plating onset at 0.05% irreversible Li for a graphite electrode with loading of 3.75 mAh/cm^2, outside the loading range of the study in Fig. 2, within 5% SOC at moderate temperatures (30 °C) and rates (3.5-5.5C). The dotted lines are the average experimental universal Li plating curve from Supplementary Fig. 12 shifted by the predicted onsets.

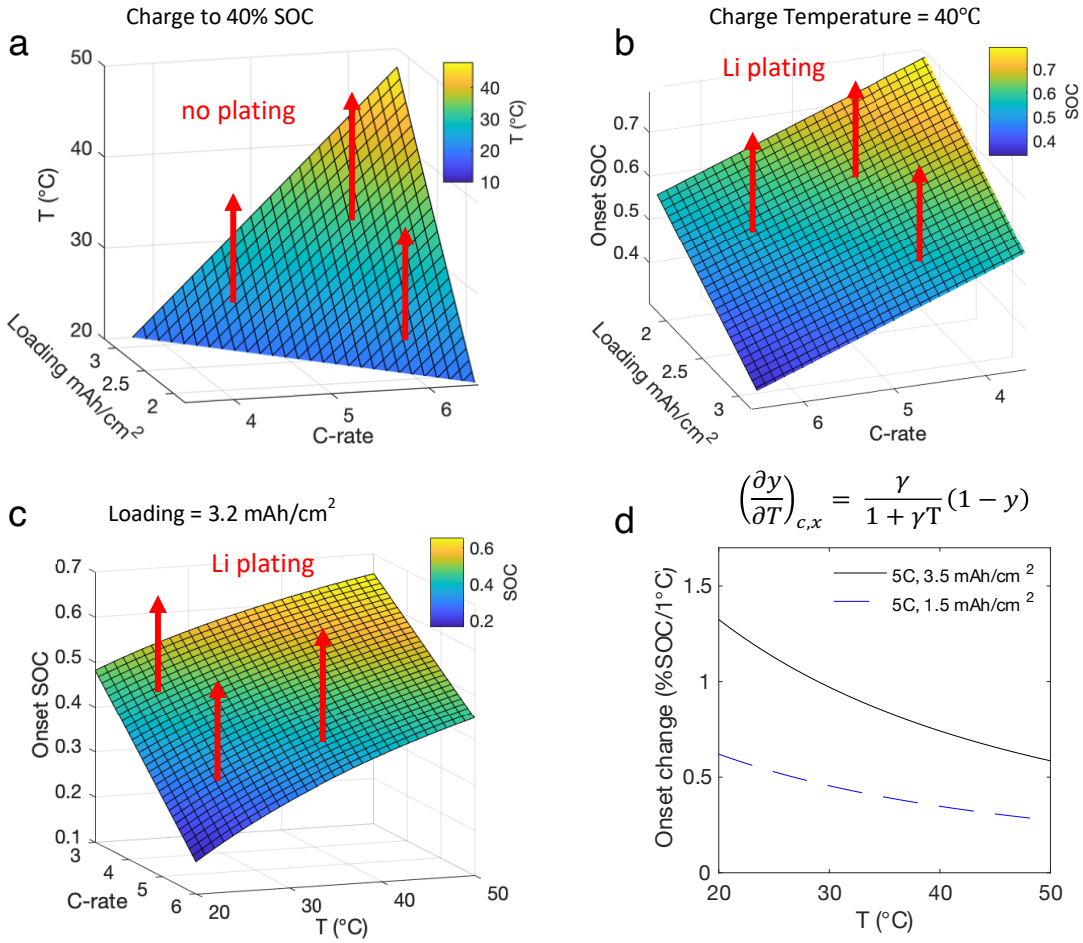

Supplementary Fig. 14 | Additional applications and insights from data-driven fitting for Li plating onsets
a) The charging temperature required to avoid plating for a constant-current (CC) charge to 40% SOC for various combinations of rates and loadings. b) Design tradeoffs to avoid lithium plating if the optimal charging temperature were fixed at 40°C, or c) if the graphite loading was required to be 3.2 mAh/cm^2 (middle). d) Another insight from the experimental data of Fig. 2g is that temperature has a smaller effect on the Li plating onset for the thinner electrodes with onsets at high SOC. The empirical fitting can quantify this effect to inform systems-level energy efficiency tradeoffs. Part d, for example, shows that as the charging temperature is increased, there are decreasing returns for postponing the Li plating onset. This analysis also quantifies the temperature effect on Li plating, and it is clear the effect is much larger for the high-loading (3.5 mAh/cm^2) curve.

$$y(c,x,T) = \frac{\alpha c + \beta x + \gamma T + \varepsilon}{1+\gamma T} \qquad (1)$$

Supplementary note 1 | Empirical fitting limitations from Manuscript Eqn 2, Fig. 2h, Table 1

In general for this empirical fitting, it is not advisable to extrapolate results more than ~30% outside of the experimental parameter range. We explain the following limitations of model application for transparency, but emphasize that this fitting is to demonstrate the utility of large Li plating data sets, so if any significant extrapolation of the data is desired, researchers should be able to collect data for those conditions and construct their own model.

Temperature. In the limit of high temperature ($T \to \infty$), the plating onset, y, goes to 1, indicating no lithium plating. This makes physical sense but does not take into account electrochemical or SEI degradation reactions that would increase at high temperature. For low temperature, at 4C rate and 3.0 mAh/cm^2 loading, non-physical

negative y values are predicted for (T < -5°C), suggesting that model calculations within ~10°C of that limit, T < 5°C, should not be used. A more robust model may use a different temperature scale or a dimensionless temperature with respect to the electrolyte freezing point, which may be a suitable limit for the plating onset truly being 0, but this is beyond the scope of the work. **C-rate.** Physically, as ($c \rightarrow 0$) the Li plating onset should go to 100% SOC. For 3.0 mAh/cm^2 loading and 30°C, the onset goes to 85% SOC, so only C-rates within the experimental range or close to it should be used. For these conditions, reasonable Li plating onsets may be expected up to 8-9C. **Loading.** Physically, as ($x \rightarrow 0$) the Li plating onset should go to 100% SOC. For 4C rate and 30°C, the calculated onset for 0 loading is 104% SOC, which is not far off. Supplementary Fig. 13 experiments also suggest that 30% extrapolation of this parameter to higher loadings (3.75 mAh/cm^2) is effective, so we expect x within the range of approximately 1.2 to 4.0 mAh/cm^2 to give reasonable Li plating predictions.

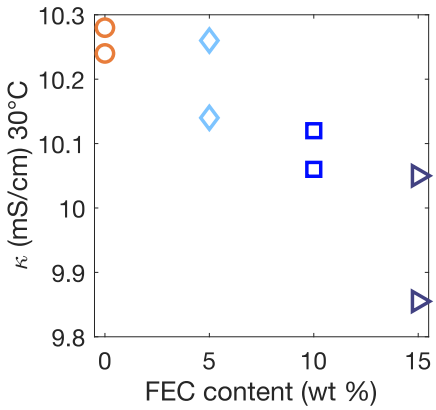

Supplementary Fig. 15 | Conductivity of carbonate electrolytes with varied FEC solvent content

Electrolyte solution conductivity data for 1.2 M $LiPF_6$ electrolyte with 0 to 15 wt% (X) FEC solvent, with total solvent wt% ratios of X:(30-X):70 FEC:EC:EMC. Conductivities were measured inside the glovebox using a Mettler Toledo InLab 751-4mm conductivity probe with blocking platinum electrodes. The probe was calibrated using 84 µS/cm, 1413 µS/cm, and 12.88 mS/cm aqueous standards (Mettler Toledo) prior to bringing inside the glove box. Electrolyte samples were maintained at 30°C using a dry block (Torrey Pines), and solution temperatures were verified using a temperature sensor inside the conductivity probe and were always within 0.2°C of the set point. Each datapoint corresponds to an independent preparation of that electrolyte; two electrolytes were made for each concentration.

Supplementary Table 4 | Baseline graphite intercalation cycle coulombic efficiencies (CE_{int}) for plating reversibility experiments

The number of baseline cycles, n, does not match the number of cells because some cells (3 for each electrolyte group) underwent 2 baseline cycles.

Electrolyte	Baseline CE (%)
70:30 EMC:EC	99.70 ± 0.11 (n=10, 7 cells)
70:25:5 EMC:EC:FEC	99.69 ± 0.03 (n=13, 10 cells)
70:20:10 EMC:EC:FEC	99.70 ± 0.03 (n=12, 9 cells)
70:15:15 EMC:EC:FEC	99.72 ± 0.04 (n=12, 9 cells)

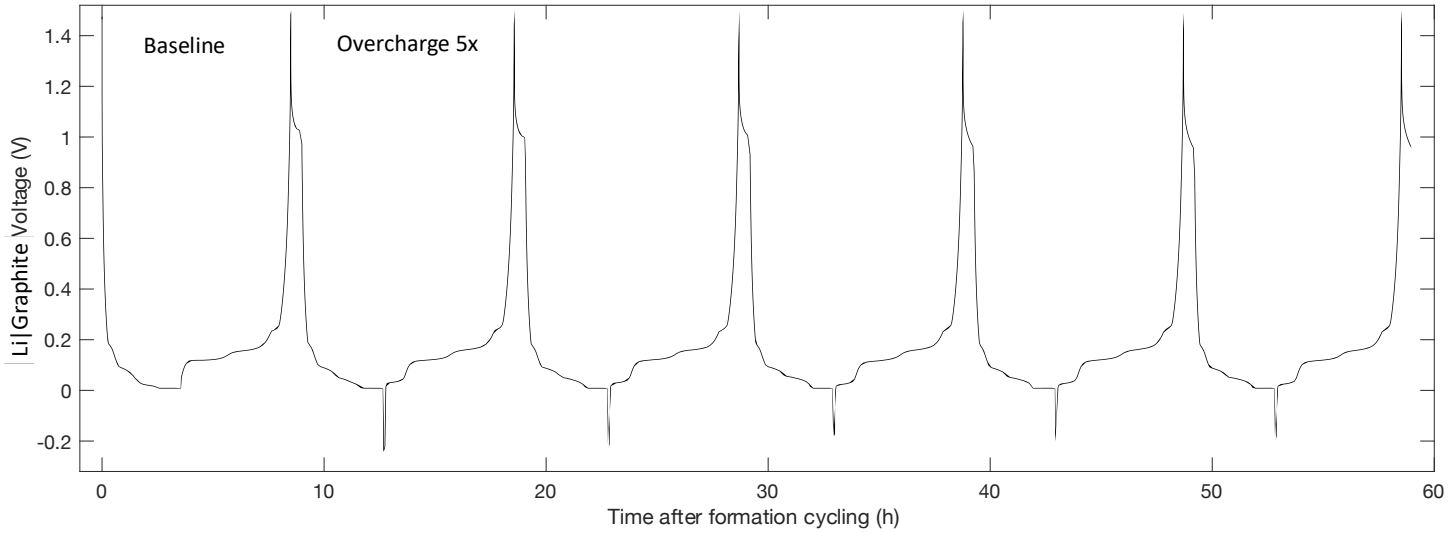

Supplementary Fig. 16 | Voltage vs time for representative Li plating reversibility on graphite experiment

Voltage profile vs. time after formation cycling for the 0% FEC cell that underwent 2C rate overcharge to 20%, the reversibility data for which is shown in Fig. 3c, Supplementary Fig. 17 bottom right plot.

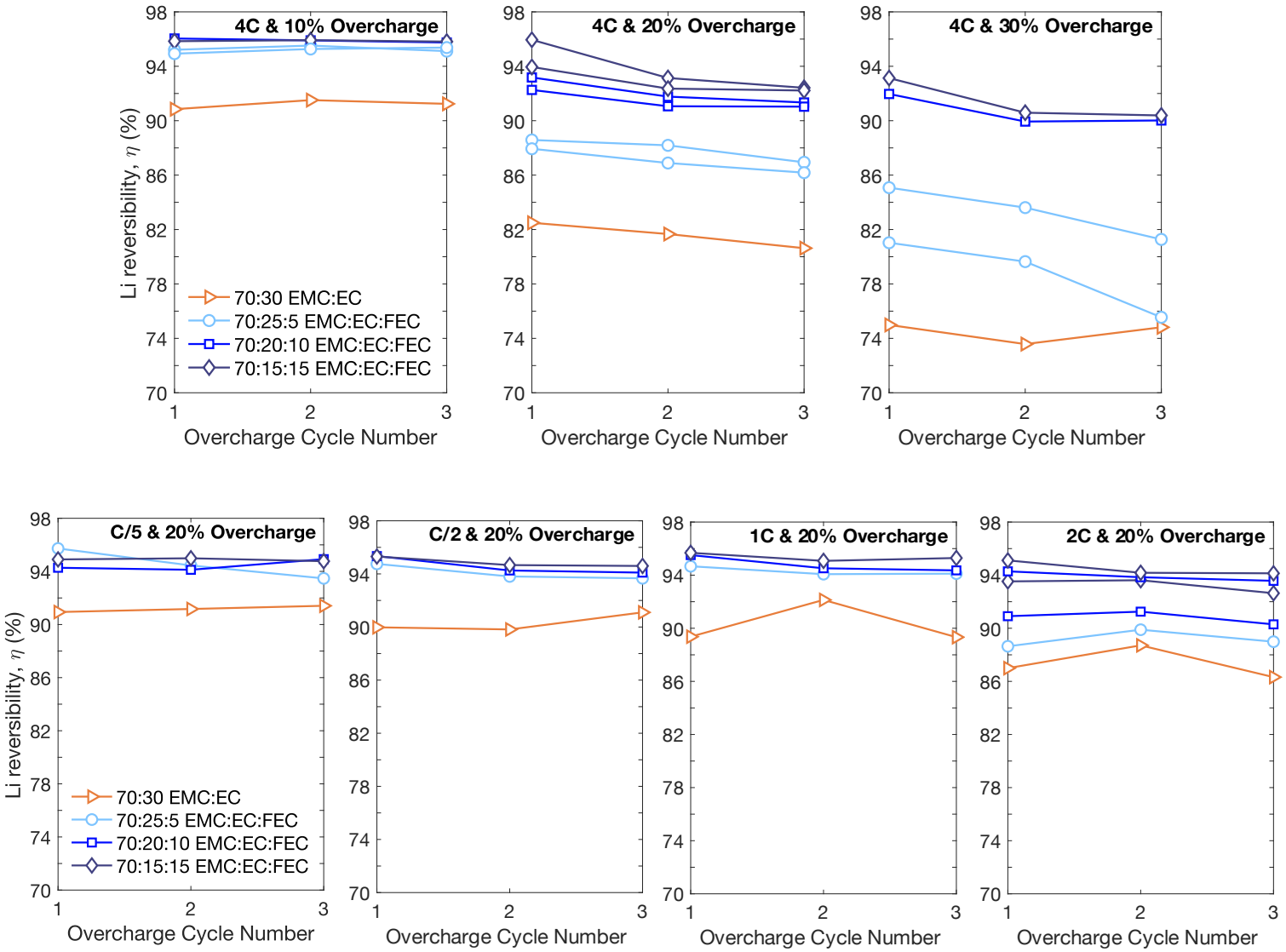

Supplementary Fig. 17 | Plating reversibility data from Fig. 3c dependence on overcharge cycle number
Calculated plating reversibilities are generally very constant for the first 3 overcharge cycles. The 4C, 30% overcharge (top right plot) shows that the 5% FEC (circles) reversibilities drift slightly with cycle number, which, combined with concerns of other cell aging effects, is why averages were only taken for cycles 1-3, shown here.

Supplementary Methods: The error bars for the incremental reversibility values in Fig. 3f were obtained from standard uncertainty propagation analysis below, where the $\sigma_{\eta_{20}}$, $\sigma_{\eta_{30}}$ were determined from multiple reversibility measurements recorded on the same cell (shown in Fig. 3c, above in Supplementary Fig. 17):

$$\sigma_{\eta_{10-20}} = \sqrt{\left(\frac{\partial \sigma_{\eta_{10-20}}}{\partial \sigma_{\eta_{20}}}\right)^2 \sigma_{\eta_{20}}^2 + \left(\frac{\partial \sigma_{\eta_{10-20}}}{\partial \sigma_{\eta_{10}}}\right)^2 \sigma_{\eta_{10}}^2} = \sqrt{4\,\sigma_{\eta_{20}}^2 + \sigma_{\eta_{10}}^2} \quad (2)$$

$$\sigma_{\eta_{20-30}} = \sqrt{\left(\frac{\partial \sigma_{\eta_{20-30}}}{\partial \sigma_{\eta_{30}}}\right)^2 \sigma_{\eta_{30}}^2 + \left(\frac{\partial \sigma_{\eta_{20-30}}}{\partial \sigma_{\eta_{20}}}\right)^2 \sigma_{\eta_{20}}^2} = \sqrt{9\,\sigma_{\eta_{30}}^2 + 4\,\sigma_{\eta_{20}}^2} \quad (3)$$

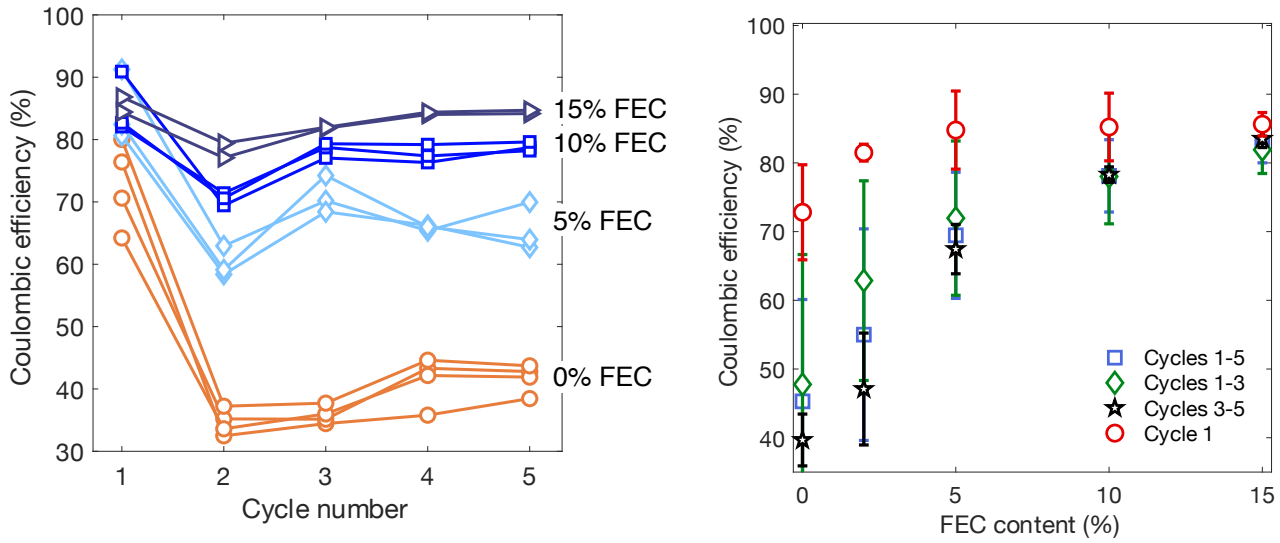

Supplementary Fig. 18 | Plating reversibility on copper foil dependence on cycle number

See Methods for cycling protocol. To make a semi-quantitative comparison of lithium plating reversibility on copper foil vs. graphite in Fig. 3f, we decided to use the average of CEs from cycles 3-5 across all cells. This is because i) we expect the graphite surface at the separator interface to be more rough than pristine foil, so the transient high CE for cycle 1, which may pertain to a unique geometry or SEI formation effect, is probably best excluded, and ii) the standard deviation for averaging cycles 3-5 better depicts the reproducibility of the data set. **Right:** To show that the trends in CE are similar with respect to FEC content regardless of which cycle numbers are averaged, the plot on the right shows average CE if cycles 1-5, 1-3, and cycle 1 are considered for averaging.

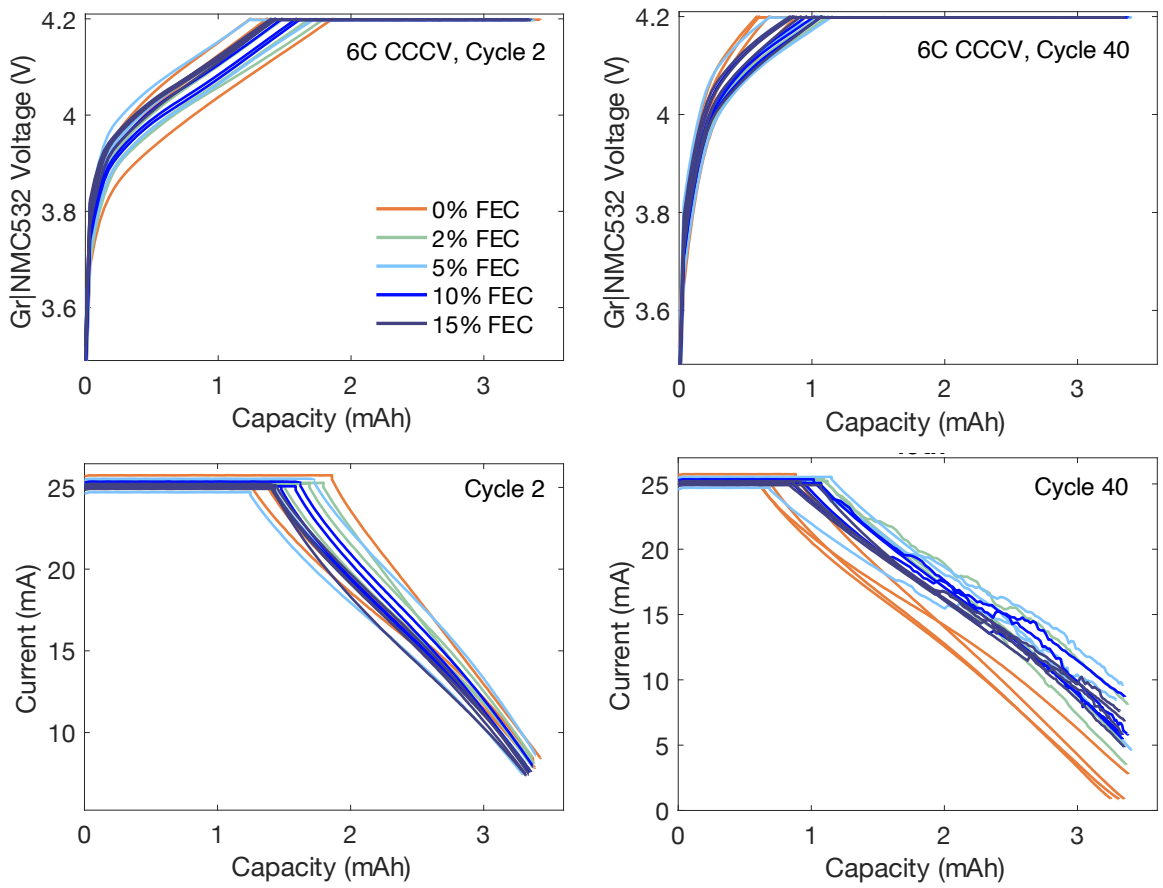

Supplementary Fig. 19 | 6C CCCV Fast charging voltage and current profiles, Cycles 2 and 40

The cell voltages and currents for the 2nd fast charge cycle of the Fig. 4a protocol (left) show experimental variability of overpotentials and current densities, included along with Supplementary Fig. 20 below to confirm that the performance enhancement with FEC is not an artefact of lower effective current densities (longer CCCV charge times). By cycle 40, Right, the effective charge rate for the 0% FEC electrolyte is lower due to the smaller CC portion of the charge, which arises from the significant loss of lithium inventory for those cells.

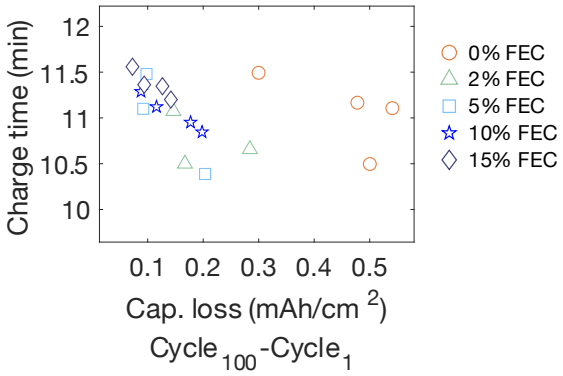

Supplementary Fig. 20 | CCCV fast charging times by FEC content

The charge times for the 2nd fast charge cycle of the Fig. 4a protocol, a metric inversely related to the average applied current density to 80% SOC during the CCCV charge, vs. the total 1C capacity loss of the cell. The times are reasonably constant across FEC concentrations, and the x-axis was selected to highlight that the poor 0% FEC performance is not explained by faster charge times (promoting more Li plating) compared to 2-15% FEC.

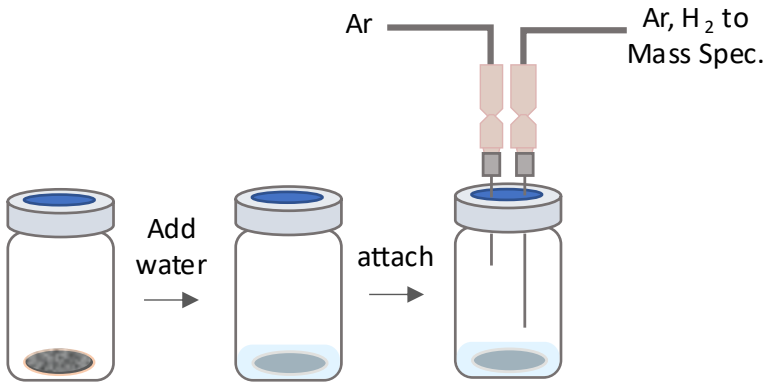

Supplementary Fig. 21 | Schematic of novel titration vial attachment method

Schematic of novel titration syringe attachment described in the Methods. Prior to each set of titrations, the system is leak tested with an in-line pressure sensor to ensure that the rate is equal to or lower than 3 Torr/min (nominal) when isolated from the gas inlet and outlet. This means that maximum 6 Torr is leaked for each 2 minute sampling period, which is less than 0.6% sample loss of the total 1030 Torr system pressure. This is an important safety and reproducibility feature. The 0.6% sample loss should be approximately constant across all vials, including the calibration data, so a correction for this is built into the calibration curve. Hamilton syringe needles with point style 5 (part # 7729-07) are used to minimize septa coring and the side port limits introduction of ambient gases during vial transfer (O_2 and N_2 mass spec signals, m/z = 32 and 28, do not increase significantly during vial swapping).

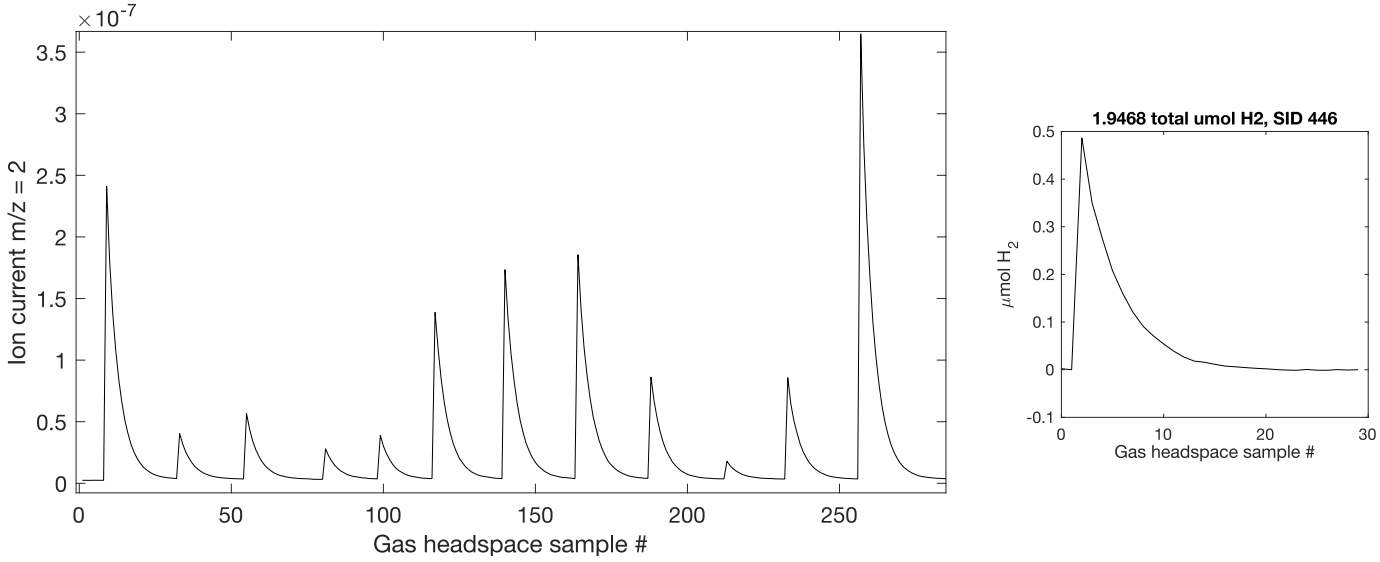

Supplementary Fig. 22 | Example titration data for vial-swapping method

Typical ion current for m/z = 2 (H_2) during a set of titrations. After ~99% decay of the signal for a given vial, the next vial is attached, resulting in a spike in the signal. The vial is typically swapped after about 20-25 gas headspace samples (every 2 min, total 40-50 min). To start the titration experiments, an empty Ar-filled vial is used to leak test and establish baseline ion current signals.

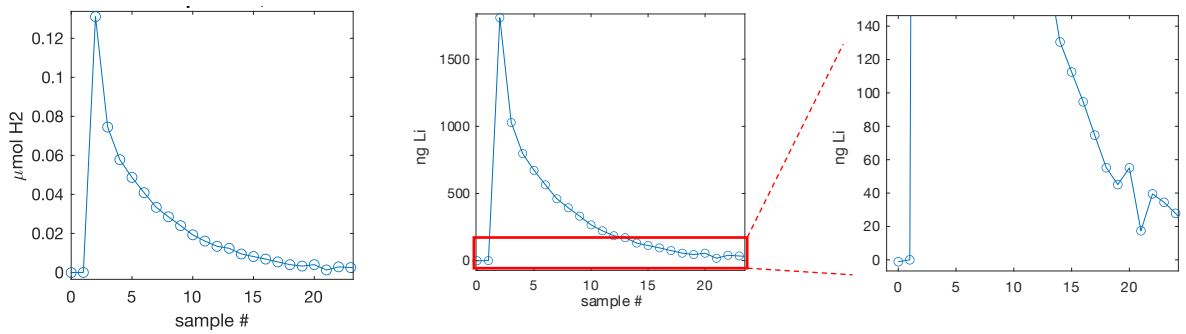

Supplementary Fig. 23 | Estimating the resolution of online Mass Spectrometry Titration for H_2, Li quantification

The left plot shows the μmol H_2 eluted in each of the 2 mL headspace samples for a total of 0.556 μmol. The middle plot is the same except with units of ng Li, obtained by multiplying the y-axis by (6.9·2·1000). Zooming in (right) shows that no significant signal noise is observed until approximately 30 ng Li, at which point still a mostly constant decrease is observed, suggesting that the resolution of the measurements is about 10 ng of Li.

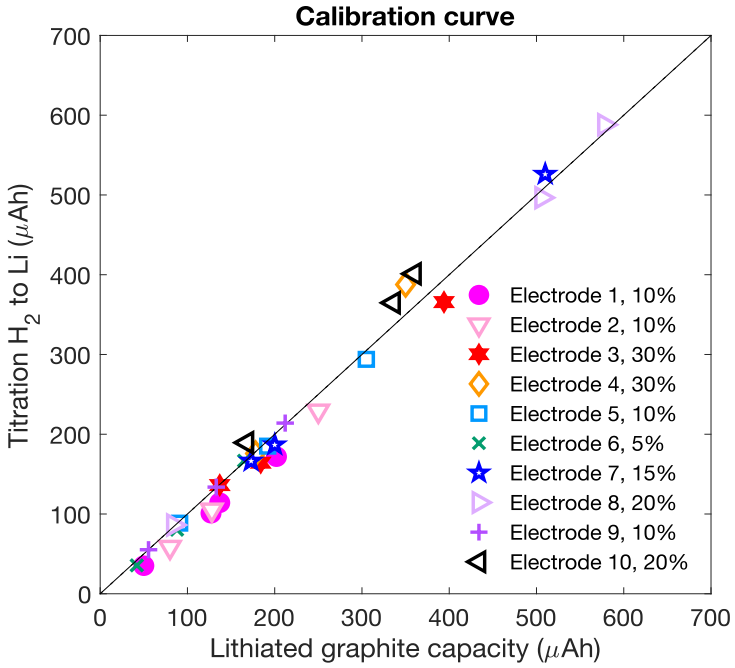

Supplementary Fig. 24 | Calibration curve generated from lithiated graphite chunks

Graphite electrodes were formed and lithiated to known SOC (10-30%) in half-cells, extracted, cut into pieces with known mass fractions of the entire 15 mm electrode, and titrated to generate the above calibration curve. Graphite pieces from the same electrode are grouped by point style. The strong linear correlation of graphite capacity with H_2, independent of graphite SOC or rinsing (filled data points were rinsed), suggests that quenching lithiated graphite is a high fidelity method for generating known amounts of H_2, and is not significantly affected by sample handling. The fluctuation around the y=x line could be due to uneven spatial lithiation of the electrode, but is not large enough to sacrifice efficiency gains by getting multiple data points per electrode. The calibration is also very consistent over months, as Electrodes 1-4 were analyzed November 2021, Electrodes 5-8 December 2021, and Electrodes 9-10 in March 2022.

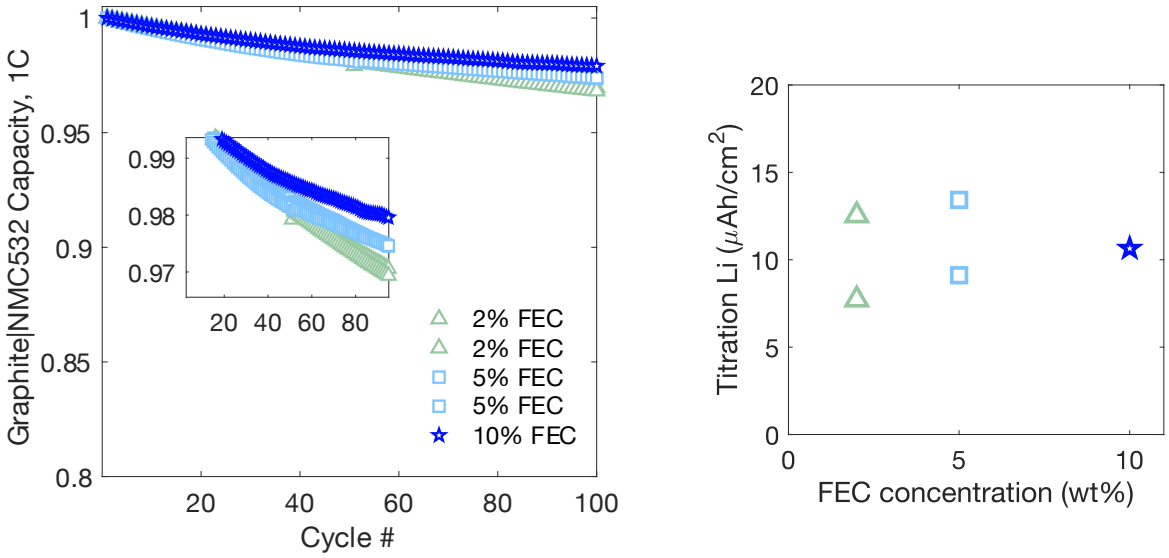

Supplementary Fig. 25 | 100-cycle 1C control experiments and titrations

Left: Only 2-3% capacity fade is observed for cells that underwent 100 1C cycles without intermittent 6C fast charging. No significant lithium plating is expected under these conditions. **Right:** Li titrated from graphite electrodes extracted from the cells in the left panel after the 100th cycle, indicating very little titrated Li, as expected. These controls averaged 10.9 ± 2.3 μAh/cm^2 (plotted with respect to 15 mm graphite electrode area, but 12.1 ± 2.6 μAh/cm^2 when normalized to active graphite material area, which is used in all other figures, see later discussion). This controls 'baseline' value is expected to be predominantly residual Li_xC_6 remaining after deep discharge and is assumed to be constant across all cells, and is thus subtracted when comparing losses ascribed to Li plating in Fig. 4c.

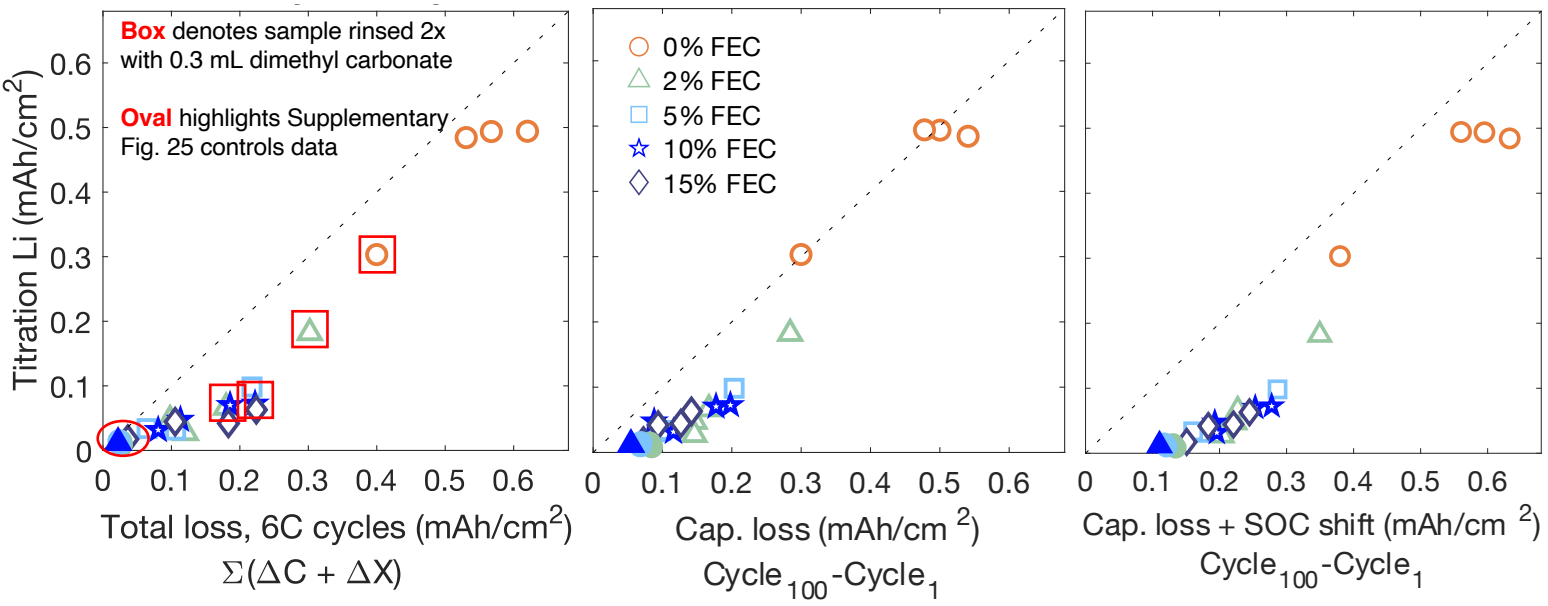

Supplementary Fig. 26 | Fig. 4c Titration Li correlation with various Cycling Data Loss Metrics

Left: This plot is the same as Fig. 4c except it shows the minimal effect of sample rinsing with dimethyl carbonate before titrations (boxes), includes the 100-cycle 1C control experiments of Supplementary Fig. 25 (filled points), and the y-values for the fast charging cells (white-filled points) are not corrected by the 0.012 mAh/cm^2 controls average baseline titration Li. **Middle:** This plot contains the same titration data from the Left

plot except the x-axis is the total capacity loss observed throughout cycling, calculated from the final (100^{th}) and initial (1^{st}) 1C discharge capacities. The 0% FEC data points along or above the y=x line indicate that it is unlikely that capacity loss fully quantifies irreversible losses from plating or fast charging, given that reactive titration species such as electrically isolated Li^0 and Li_xC_6 are only one source of losses. **Right:** The combined total capacity loss and total graphite SOC shift over 100 cycles, the new x-axis, correlates strongly with Titration Li for the FEC-containing electrolytes, another indication that the graphite SOC shift is highly relevant for cell performance.

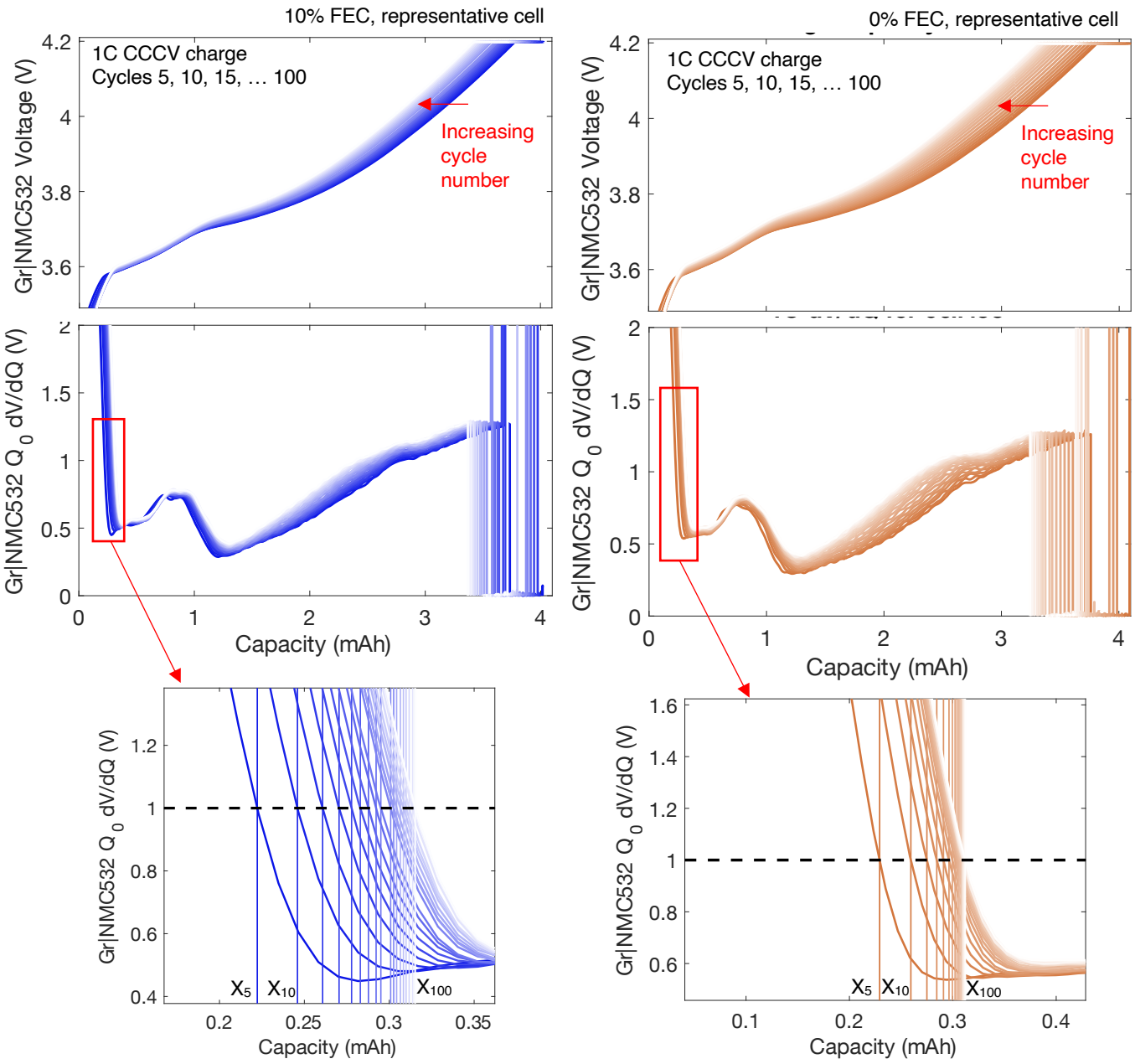

Supplementary Fig. 27 | 1C Cycle Voltage Profiles, Q_0 dV/dQ, and Calculating the Graphite SOC Shift ΔX

Top: 1C cycle charge profiles for the protocol of Fig. 4a. **Middle**: Differential voltage with respect to capacity (see Methods) for the corresponding 1C charge profiles. **Bottom:** Illustrating the methodology for quantifying the voltage segment shift corresponding to early graphite lithiation. The capacity at which Q_0 dV/dQ = 1 for each curve is shown by the horizontal lines, X_5, … X_{100}, and these values are used to calculate the Graphite SOC Shift ΔX as described in the Methods. Using this criterion to calculate curve shifts avoids the noise, error, and algorithm complexity of assigning capacities to local extrema (peaks or troughs) in the Q_0 dV/dQ curves.

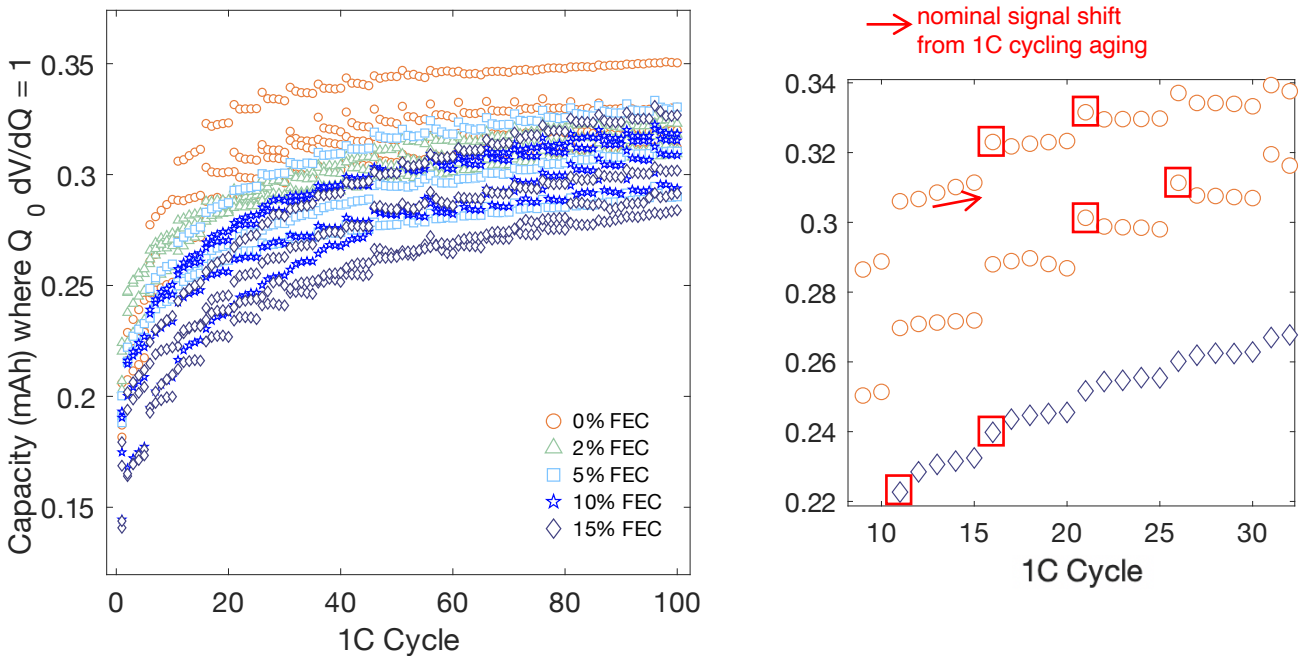

Supplementary Fig. 28 | Graphite SOC shift calculation from 1C cycles

The left plot shows capacity at which Q_0 dV/dQ = 1.0 V, denoted X_i in Supplementary Fig. 25 and the Methods (i is the 1C cycle number), for each 1C charge for all cells included in the study. The enlarged region in the right plot highlights in red boxes that the 1st 1C cycle following 6C CCCV fast charge (cycles 6, 11, 16, …) shows transient behavior, which is why the value for the 2nd 1C cycle following fast charge (cycles 7, 12, 17, …) is used for the ΔX as described in the Methods, equations below for reference. The arrow highlights nominal X_i change from 1C cycling, which is why this change over 2 cycles (from N-2 to N, below) is subtracted from the ΔX for the 2 6C cycles to distinguish contributions related to fast charging from nominal cell aging/formation.

$$\Delta X_{6C\ cycles\ 1\ \&\ 2} = (X_7 - X_5) - (X_5 - X_3) \qquad (4)$$

$$\Delta X_{6C\ cycles\ n\ \&\ (n+1)} = (X_{N+2} - X_N) - (X_N - X_{N-2}) \qquad (5)$$

For 1C cycle numbers: N = [5, 10, 15, …, 90, 95] and
Corresponding 6C cycle numbers: n = (2N/5) - 1 = [1, 3, 5, …, 35, 37]

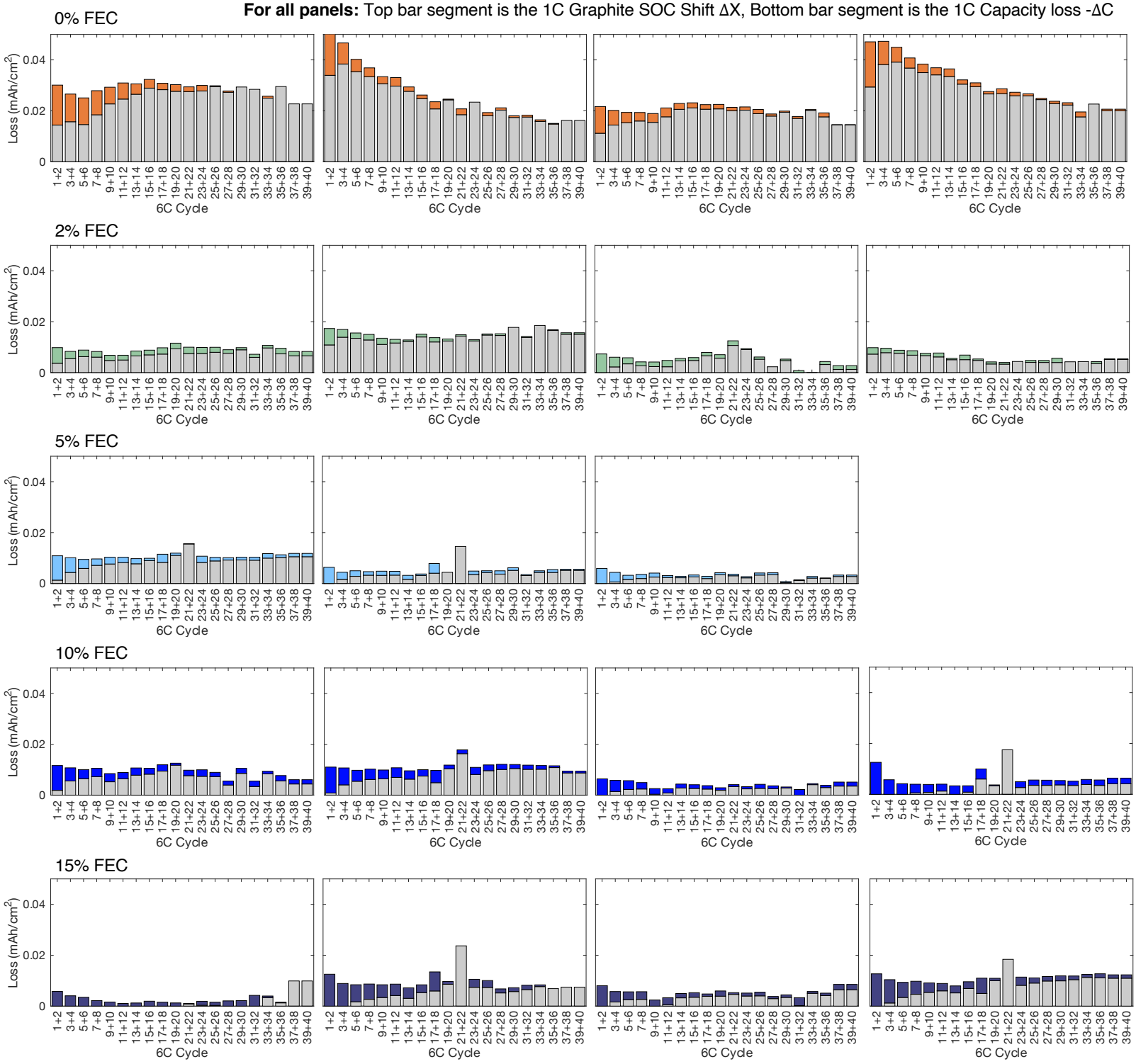

Supplementary Fig. 29 | Capacity loss and Graphite SOC shift by fast charging cycles, all cells

Plots analogous to main text Fig. 4c are shown for all individual cells studied in Fig. 4, grouped by electrolyte concentration. The combined loss of the graphite SOC shift (grey bars, bottom) and the capacity loss (colored bars, top) is remarkably constant or decreasing, as expected and described in the main text, for nearly all cells. This evidence promotes the reliability of these combined metrics to quantify fast charging and Li plating-related loss. Future work could incorporate outlier removal for plating quantification; the data blip for cycles 21+22 for a few cells is due to temporary thermal chamber temperature increase to ~32ºC at that time due to laboratory air conditioning maintenance, when the warm ambient air makes it difficult to cool the oven temperature to 30.0 during heating-only operation.

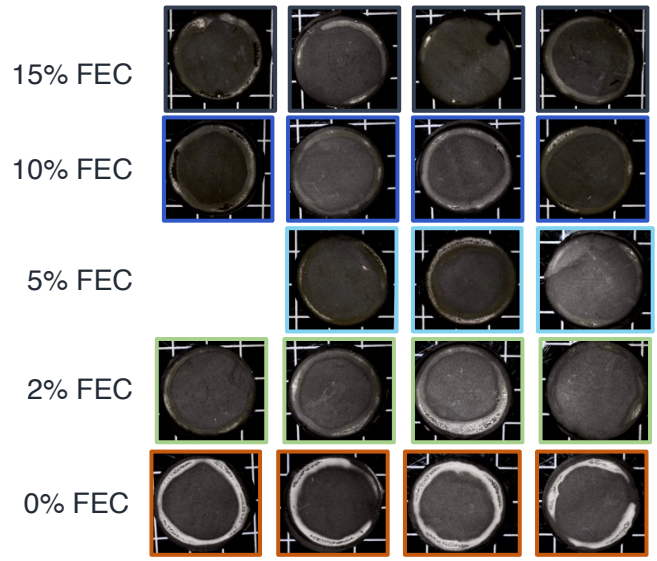

Supplementary Fig. 30 | Graphite electrode images before mass spectrometry titrations

The 0% FEC electrodes from Fig. 4 experiments show much more prominent metallic lithium, motivating the desire to quantify the amounts with titrations. These images also confirm that plating is occurring on the graphite electrode, and not on the spacers behind it, a testament to good electrode alignment and cell fabrication. We believe that the ring shape of plating is due to higher current densities passed near the edge of the undersized NMC electrode (14 mm vs. 15 mm graphite), and is not (at least primarily) a pressure effect from the coin cell spring.

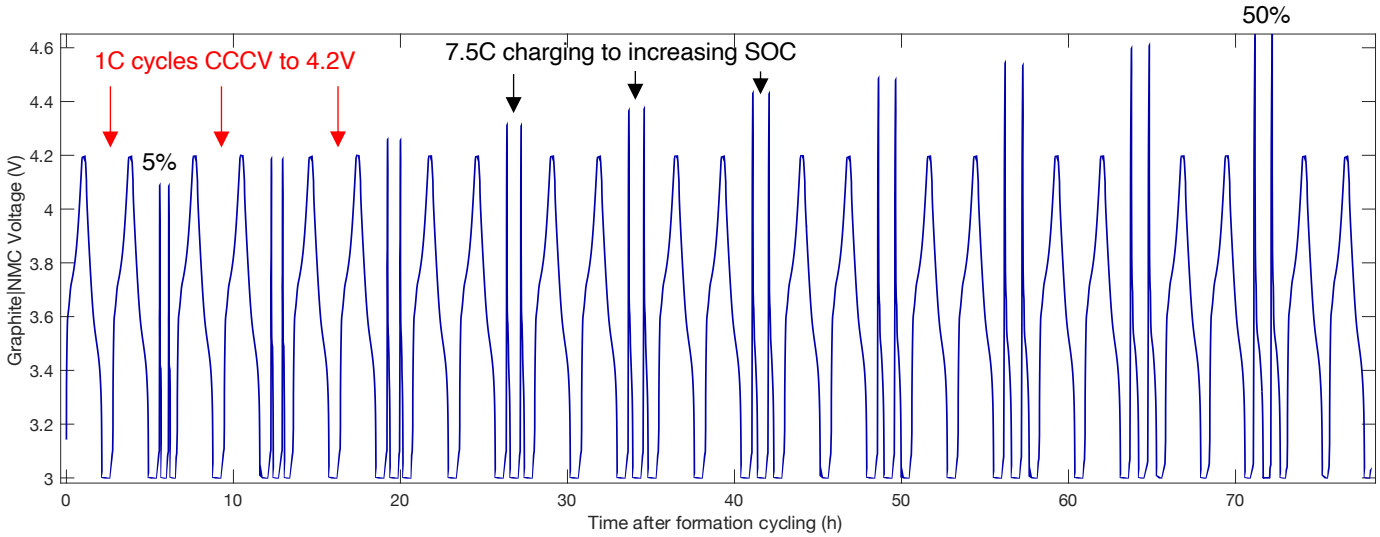

Supplementary Fig. 31 | Gr|NMC voltage during SOC-sweep cycling protocol

This figure illustrates the protocol of alternating 1C cycles with fast charging cycles to different SOC cutoffs, described in the main text and Methods. This data corresponds to 7.5C fast charging ranging 5% SOC (first cycles) to 50% SOC (last cycles).

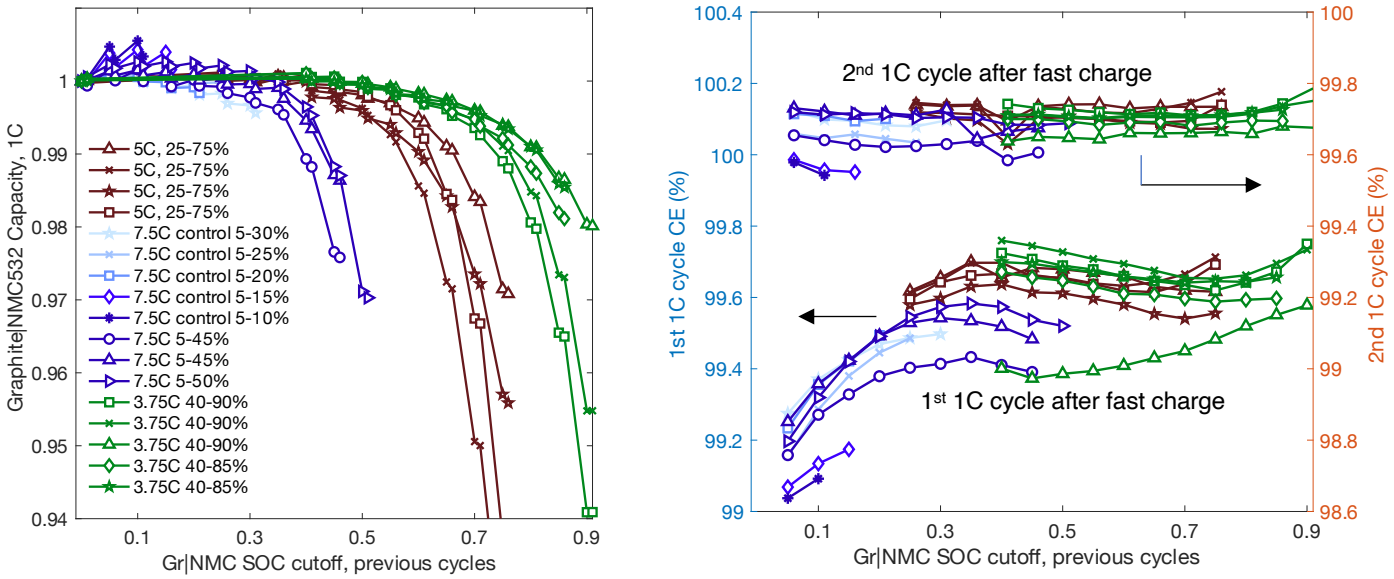

Supplementary Fig. 32 | SOC-sweep 1C discharge capacities and coulombic efficiencies

Left: Main text 5a plot including data from all cells (each unique curve). For many curves, there is significant capacity change observed within each pair of 1C cycles (adjacent points), which is unexpected from previous 100-cycle experiments. We believe the 1C cycle immediately after fast charge has transient anomalous behavior, which was also seen and discussed for the similar protocol in Supplementary Fig. 30, and thus only the 2nd cycle of each pair was used for quantitative analysis. **Right:** The 1C cycles immediately after the fast charging pair (bottom) show drifting CE values between 99.2-99.7% throughout cycling. The 2nd cycle after fast charging (top) shows fairly stable CE between 99.6-99.8%, suggesting stabilized cell behavior desirable for precise discharge capacity analysis.

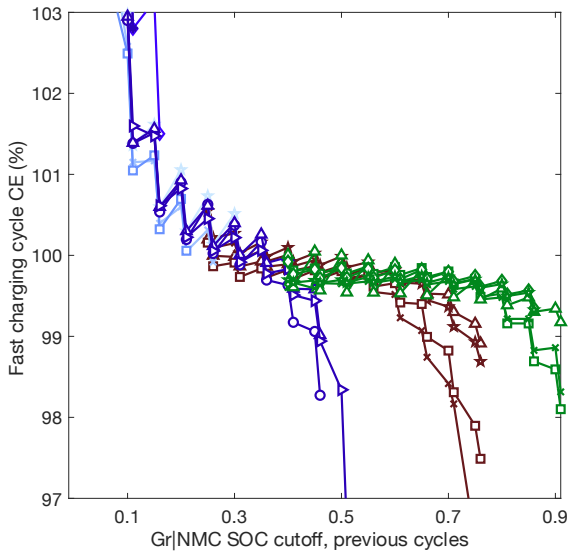

Supplementary Fig. 33 | SOC-sweep fast charging cycle coulombic efficiencies

This plot shows the intermittent fast charging cycle coulombic efficiencies corresponding to Supplementary Figs. 31-32 and 5. Unlike the CE's used to quantify irreversible Li plating in in Li|Gr cells, these values can frequently be greater than 100% and do not exhibit a stable baseline (as in Supplementary Fig. 1) prior to a decrease that indicates the clear onset of irreversible plating. This highlights the benefit of the stable potential of lithium counter electrode in half-cells and is why the 1C cycle discharge capacities and graphite SOC shift are analyzed instead of the fast charging cycles.

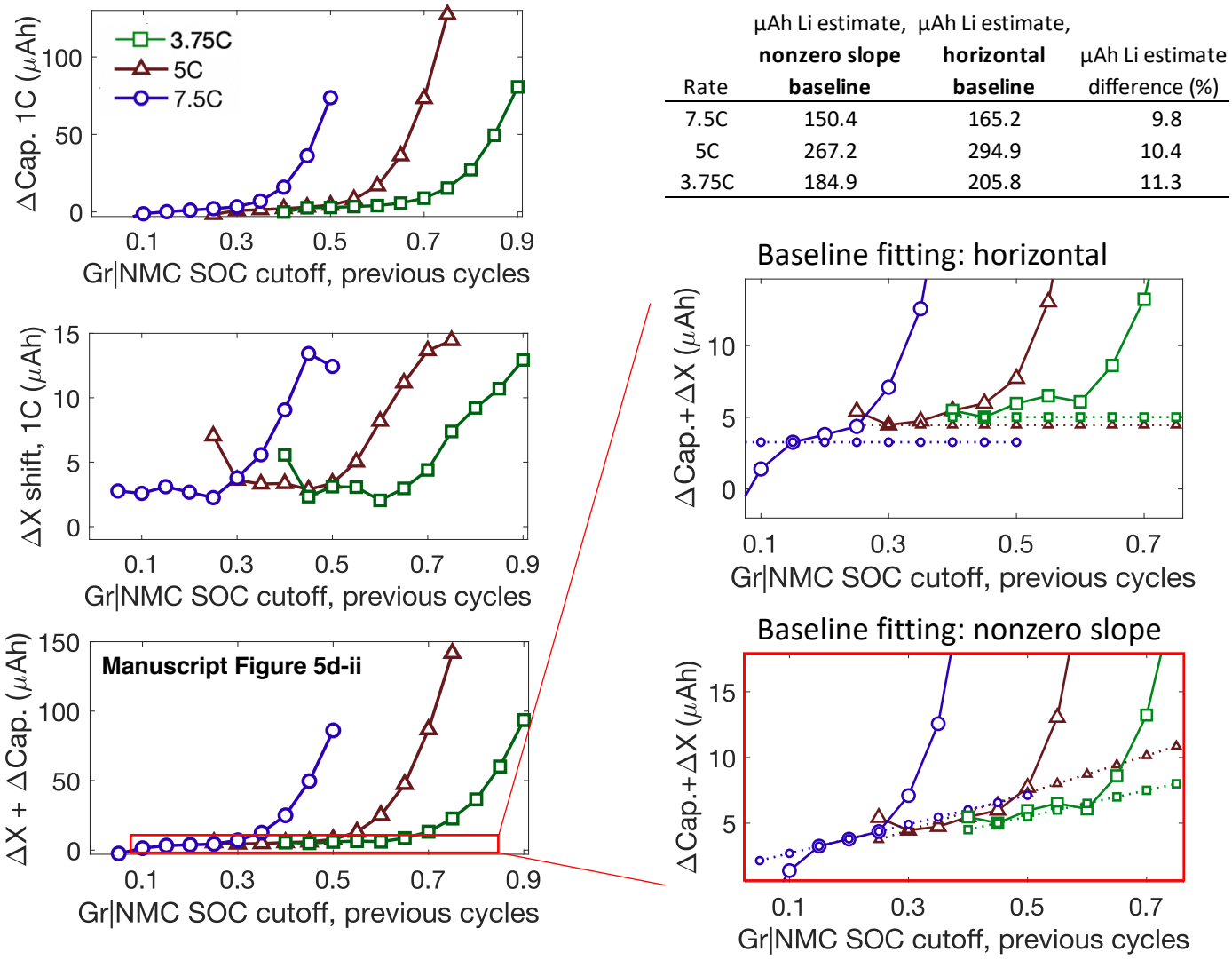

Rate	μAh Li estimate, **nonzero slope baseline**	μAh Li estimate, **horizontal baseline**	μAh Li estimate difference (%)
7.5C	150.4	165.2	9.8
5C	267.2	294.9	10.4
3.75C	184.9	205.8	11.3

Supplementary Fig. 34 | Estimating irreversible Li from ΔX and ΔC obtained from the SOC-sweep protocol

Left: The individual contributions of capacity loss (ΔC) and graphite SOC shift (ΔX) to the combined loss shown in Fig. 5a. Interestingly, ΔX alone also shows a clear increase at the SOC where the onset of lithium plating is expected, but with lower sensitivity than ΔC (note ~10^1 y-axis scale difference). However, these contributions are significant for quantifying total irreversible lithium plating. **Right**: To isolate irreversible lithium plating from other nominal cell degradation, we subtract baseline losses for each (ΔC+ΔX) data point using a linear baseline with slope > 0 that passes through the data points at low SOC. Each cell (dotted lines) has a unique baseline with nonzero slope, shown in the red box. This baselining protocol is conceptually equivalent to the previous half-cell CE baselining, which instead uses a singular CE value, because the capacity loss is scaled by the charge capacity by definition of the coulombic efficiency. Figure S35 below illustrates this point by recasting half-cell data into capacity loss units instead of CEs. Physically, this means that most experimental cells herein exhibit an SOC-dependent fast charge aging likely related to continued graphite SEI formation or electrode de-wetting, but also possibly related to counter electrode (NMC or Li) performance, beyond nominal aging such as that from the 2 1C cycles for this SOC-sweep experiment.

To gauge the sensitivity of the cumulative irreversible plating estimate (Fig. 5c, x-axis) to baseline fitting, we calculate this plating estimate for the extreme case of a horizontal baseline that has no SOC-dependence on nominal cell aging (middle) and show the values in the table. Using the horizontal baseline gives an

approximately 10% overestimate for the plating amount across these representative cells, suggesting this is the maximum possible error due to baseline fitting. However, the control experiments in Supplementary Fig. 36 show no titration Li below 0.3 SOC for the 7.5C charging, suggesting no irreversible Li plating, which further supports the nonzero slope baselining approach that gives zero irreversible plating at those SOC in addition to the half-cell justification. From this discussion, we believe the baseline fitting error of irreversible Li quantification is much smaller than 10%, likely in the range of 2-3%.

Finally, the baselined data were then divided by 2 (2 fast charging cycles to each SOC), and normalized to the active graphite capacity, $C_{active\_graphite}$ (5.24 ± 0.07 mAh determined from dV/dQ analysis of 5 cells, Supplementary Fig. 37). The irreversible Li values at low SOC were set to 0 to remove data noise artefacts, and the cumulative Li plating capacity estimate (x-axis, Fig. 5c) excluded these points.

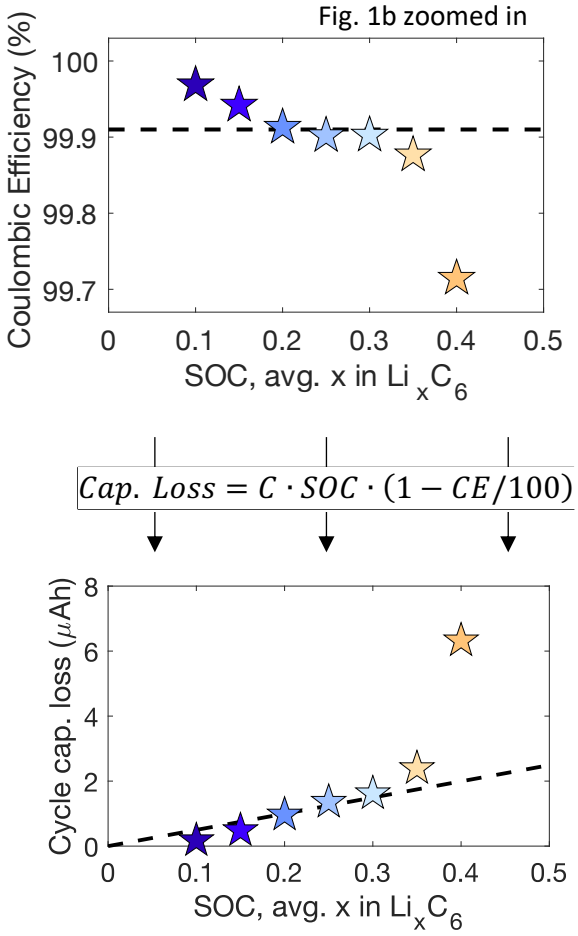

Supplementary Fig. 35 | Half-cell CE baselining for SOC-sweep protocol recast in irreversible capacity units

Converting the CE data of Fig. 1b (top) to capacity loss (bottom) illustrates how using a horizontal baseline for CE analysis [y = 99.91] is equivalent to using a nonzero slope baseline with capacity units [y = C·SOC·(1-0.9991)], where C is the experimental cell capacity. This further justifies the use of a nonzero slope capacity baseline for the full-cells plating analysis, in which coulombic efficiencies for the fast charging cycle cannot be analyzed due to unpredictable artefacts seen in Supplementary Fig. 33.

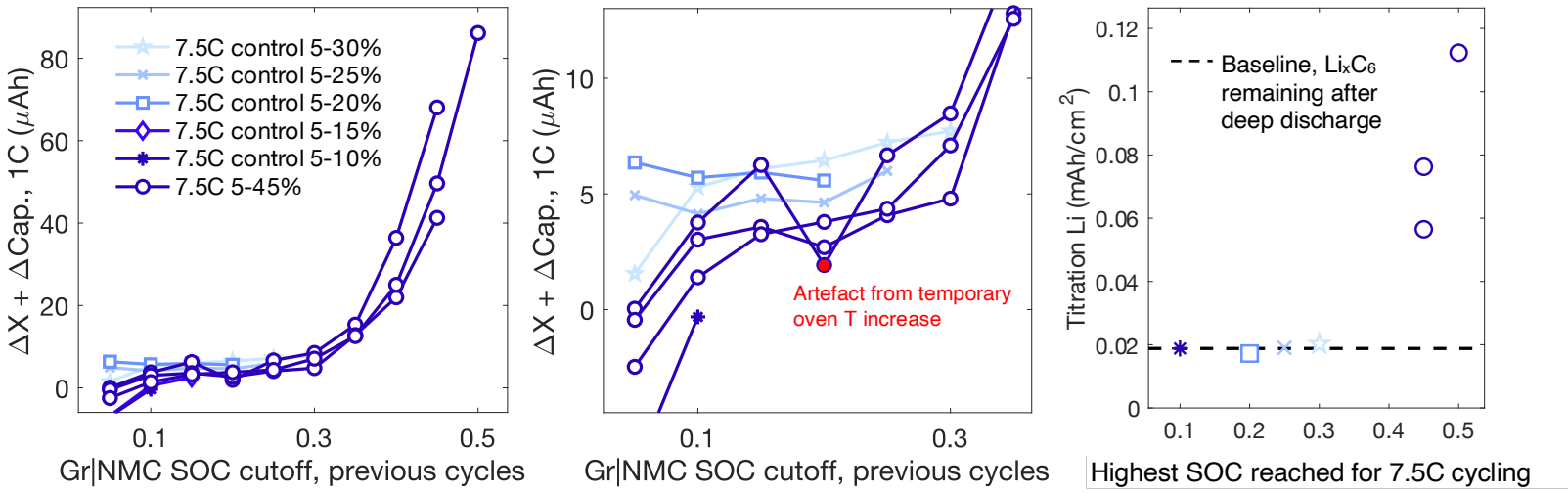

Supplementary Fig. 36 | SOC-sweep control experiments: titration results for cycling at 7.5C to low SOC

Left: (ΔX+ΔC) data for all 7.5C fast charging cells, including control experiments that started cycling at 5% SOC but were stopped at various points during the protocol. **Middle**: Zooming in on the left data shows that the control cells also show the characteristic increase in (ΔX+ΔC) capacity with continued cycling to higher SOC. The filled data point, collected when the oven temperature fluctuated up to ~32ºC from 30ºC, emphasizes the importance of temperature control for precisely quantifying small amounts of irreversible lithium. **Right:** The titrated Li for these cells shows a very constant baseline (dashed line) that should correspond predominantly to Li_xC_6 remaining after the deep discharge step of the protocol. This value is 0.019 ± 0.001 mAh/cm^2, and the cells with significant expected irreversible Li (circles) show titrated Li much greater than the baseline.

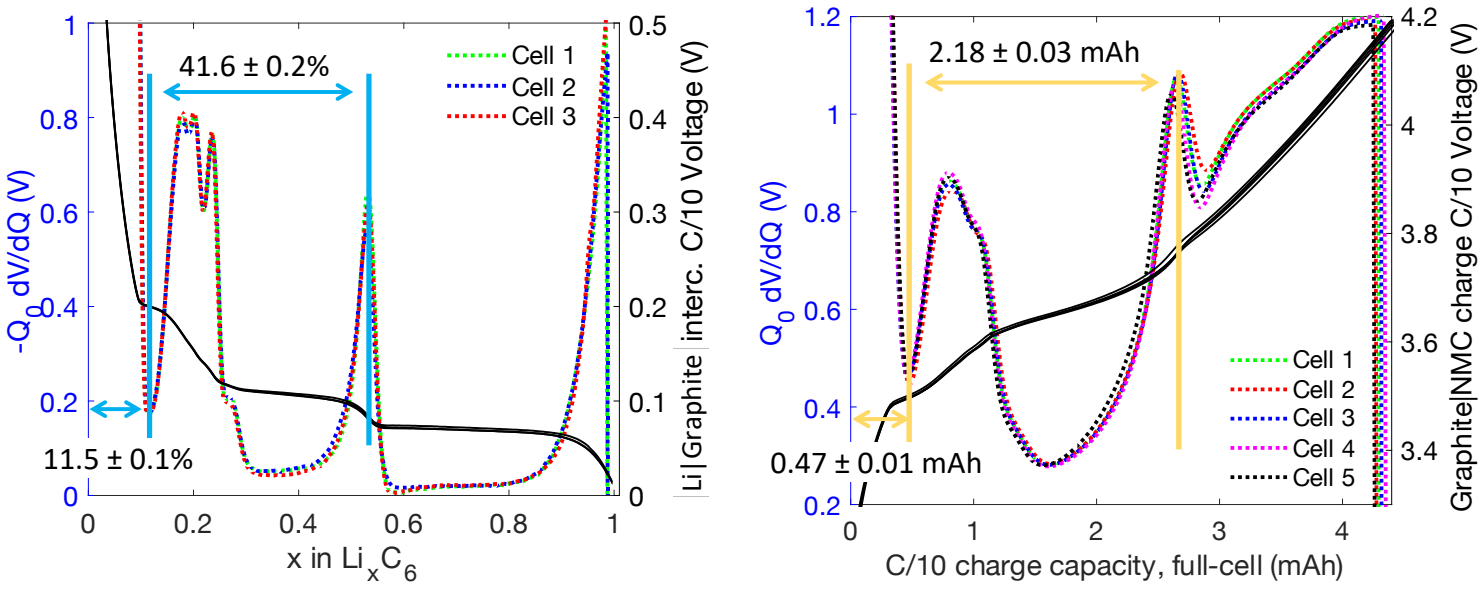

Supplementary Fig. 37 | Using dV/dQ analysis to determine active graphite capacity and lithiation in full-cells

Left: C/10 intercalation voltage (black) to 0.01 V for the 3rd C/10 formation cycle of 3 representative Li|Graphite cells, using the graphite electrode A3 (see Materials section in Methods) and 0% FEC electrolyte. The capacity is normalized to 1 (x-axis). The average normalized capacity up to the first trough in the $-Q_0$ dV/dQ signal (dotted, colored curves) is 11.5 ± 0.1%, and the capacity between the trough and the clear peak (near x = 0.5) is 41.6 ± 0.2%. These features related to graphite phase change are also visible in the Q_0 dV/dQ analysis during full-cell charging (Right). **Right:** C/10 full-cells charging voltages (black) for the cycle immediately preceding the fast charging SOC-sweep for 5 representative cells (see Methods for protocol), overlaid with Q_0 dV/dQ. The capacity between the first trough and the clear peak (near 2.6 mAh) is 2.18 ± 0.03 mAh. Assuming similar graphite phase behavior at these low rates in the full-cells as to half cells, this amount is 41.6 % of the active graphite material, and on average, 2.18/0.416 = 5.24 mAh is the active graphite capacity in the full-cell configuration. The graphite lithiation at the start of C/10 charge (equivalently, the lithiation at the end of the 1C discharge with 3V hold until C/20) can be calculated from this value and the capacity up to the first trough, 0.47 ± 0.01 mAh, assuming that the trough corresponds to 11.5% graphite lithiation as observed in half-cells. From this, the initial average graphite lithiation in the full-cells is 2.5 ± 0.1%, calculated from (0.115*5.24 – 0.47)/5.24.

Supplementary note 2 | Calculating Gr|NMC C-rates to get the same effective graphite current densities as in Li|Gr cells

The NMC electrode in the full-cells was slightly undersized to avoid edge effects like lithium deposition on the stainless steel spacer behind the graphite electrode. To compare irreversible lithium plating in full-cells and half-cells, however, the effective current density applied to the graphite electrode during charge should be fixed. This calculation needs to take into account what area of the 15 mm diameter graphite electrode is actively lithiated and delithiated during cycling. Prior to the above analysis of Supplementary Fig. 37, the below diagram was constructed to help visualize relevant cell length scales to make a reasonable estimate for how much of the graphite 'overhang' region may be active or utilized for the case of perfectly concentric electrodes. We reasoned

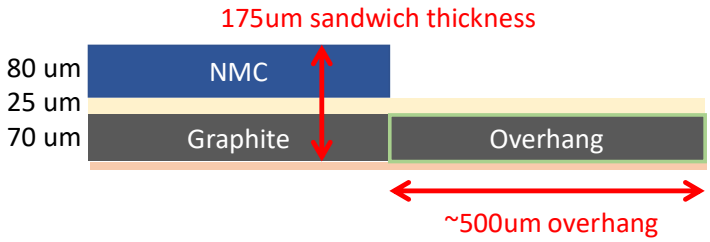

that 50% of the overhang region might be utilized, or 14.5 mm of the 15 mm diameter graphite in total, due to expecting full wetting of the electrodes and separator with electrolyte. From this assumption and knowledge of the average observed capacity for 15 mm A3 graphite in the half-cells, 5.90 mAh, we multiplied this by the area ratio of (14.5 mm dia.)/(15 mm dia.) = 0.934 to estimate there is 5.5 mAh active graphite in the full-cells. In other words, if the 1C rate in half-cells is 5.9 mA, then the equivalent total current used in the full-cells should be 5.5 mA. Finally, the average full-cells experimental capacity based on the 3rd C/10 formation cycle to 4.2V was 4.30 mAh, indicating that the 1C rate in full-cells is 4.30 mA, so to get the desired 5.5 mA corresponding to 1C rate in half-cells, the full-cell rate should be multiplied by a factor of (5.5/4.3) ~ 1.25. This factor was used to select full-cell rates [3.75C, 5C, 7.5C] corresponding to [3C, 4C, 6C] rates in the half-cells in Fig. 5.

However, after the Supplementary Fig. 37 analysis, a more accurate estimation of the active graphite material was determined to be 5.24 mAh compared with the 5.5 mAh calculated from the 50% overhang utilization assumption. Imaging the graphite electrode after C/10 lithiation to 4.2V in the full-cells also shows significant overhang region that does not show the gold-colored LiC_6 (see image below), giving support for the fidelity of the dV/dQ analysis capacity of 5.24 mAh (instead of 5.9 or 5.5 mAh), which would correspond to only a ~14.2 mm diameter circle of the graphite being utilized. This means that the graphite current densities in the full-cells are likely (1-5.24/5.5) = 5% higher than those applied in the half-cells due to error in the 1.25 factor used to convert between C-rates. This offset is significant but not expected to affect the trends and conclusions drawn in the Fig. 5e comparison of half- vs. full-cells, because the empirical fitting from Eqn. 2 and Table 1 indicates that a 5% change in current rate for the half-cells will only affect the plating onset SOC by ~2% for a 3.25 mAh/cm^2 electrode with 4C rate at 30 ºC.

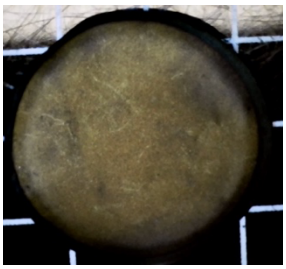

After C/10 lithiation to 4.2 V in full-cell

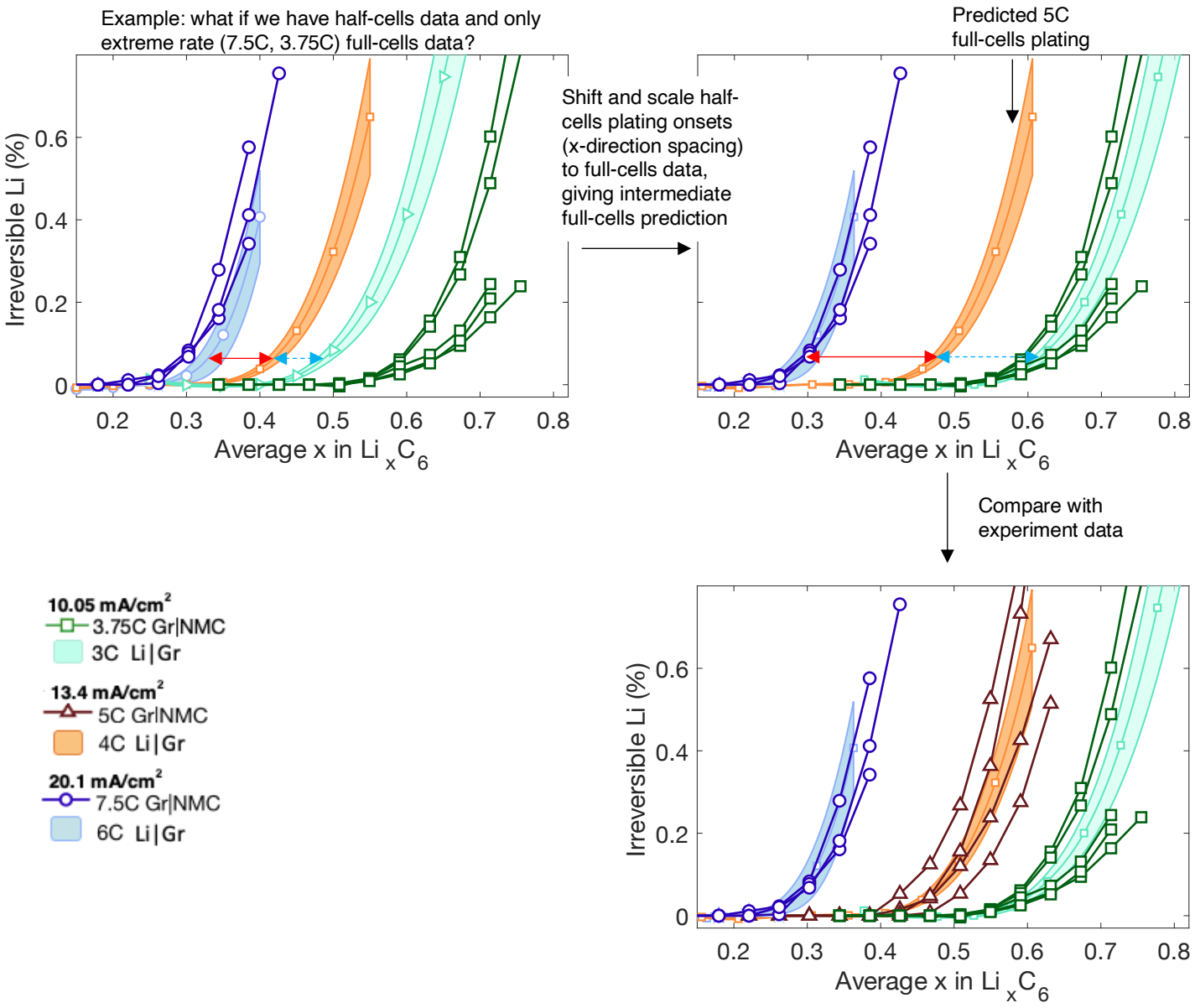

Supplementary Fig. 38 | Scaling half-cell irreversible Li plating data to predict full-cell data with limited measurements

Top Left: Replicated Fig. 5b except without the 5C Gr|NMC full-cells data. In all panels, the experimental Gr|NMC data is fixed and shown for reference/comparison. The SOC spacing between the half-cells data (arrows) is scaled such that the spacing between 3C and 6C becomes the same as the spacing between full-cells 3.75C and 7.5C. The curves are then shifted so that the corresponding half/full-cell extremes overlap (3C with 3.75C, 6C with 7.5C), and this transformation result is shown in the **Top Right** figure. The scaled 4C half-cell curve (shaded orange) is now a prediction for Li plating at 5C rate in the full-cells. **Bottom:** Overlaying the 5C full-cell experiment data shows excellent match with the half-cell-based prediction, suggesting that half-cells data and models may be adjusted to predict full-cells behavior with limited full-cells data to provide corrections. For this analysis, plating onsets were again defined as the average x-value where the curves cross the y=0.05 threshold.

Supplementary note 3 | Understanding the observed differences in half-cells and full-cells

The differences for lithium plating onset between full-cells and half-cells is multifaceted. At high current densities, the full-cell plates lithium at lower SOC compared to half-cells. Conversely, at moderate current densities, the half-cell plates lithium at lower SOC compared to full cells, which is somewhat unexpected. A detailed electrochemical model was run in full-cell configuration using NMC properties previously reported[9], and the same complex behavior is predicted for lithium plating onset when comparing configurations. Upon studying model results, the earlier onset for half-cells at moderate current densities seem to be related to the functional form of electrolyte properties with concentration and the relatively flat open circuit potential for graphite. The electrolyte potential drop, which effects SOC heterogeneity, is a function of both electrolyte ionic conductivity and diffusivity. During charging, ion concentration drops in the anode. This results in a decrease in ionic conductivity but an increase in diffusivity. The ion concentration in the anode during charging is lower in full-cells compared to half-cells. At moderate rates, the full-cell seems to be delayed in lithium plating compared to half-cells due to gains in electrolyte diffusivity outweighing a slight drop in ionic conductivity (Fig. 1 in Ref 9). However, at high current densities, lithium plating occurs earlier in full cells because severe ion depletion occurs more and the ionic conductivity for large sections of the anode goes to zero. Thus, decreases in ionic conductivity outweigh gains in diffusivity at high current densities when comparing cell setups.

Supplementary Table 5 | Cell Counts by Experiment type

Experiment type	Figure Number	Number of Cells
Li|Gr SOC-sweep, effects of T, loading, rate	2a-f	61
Li|Gr SOC-sweep, high-loading electrode	S13	5
Li|Gr SOC-sweep, for full-cell comparison	5b	8
Li|Gr SOC-sweep, FEC effect	3a	12
Li|Gr single SOC per cell, 25C control expts.	S2	12
Li|Gr single SOC per cell, 45C controls	S6	16
Li|Gr plating overcharge, reversibility studies	3c	35
Cu|Li high-rate plating FEC effect	3e, S18	12
Gr|NMC 6C plating FEC effect	4a,b	18
Gr|NMC 1C 100-cycles control experiments	S25	5
Gr|NMC Li plating quantification	5b	12
Gr|NMC Li plating quantification, controls	5c, S36	4

Supplementary note 4 | Calculating the Li:Gr molar ratio of half-cells and influence on performance

The median graphite electrode loading used in this work was 3.1 mAh/cm^2 , which has capacity of 5.5 mAh for a 15 mm diameter punch. The lithium metal used was a 14 mm diameter punch (1.54 cm^2) with 0.75 mm thickness. Thus, the total theoretical capacity of the lithium metal electrode is:

$$(0.075\ cm\ thick) \cdot (1.54\ cm^2\ area) \cdot \left(0.5 \frac{g\ Li}{cm^3}\right) \cdot \left(\frac{1\ mol}{6.9\ g\ Li}\right) \cdot \left(96485 \frac{C}{mol\ e^-}\right) \cdot \left(\frac{mAh}{3.6\ C}\right) = 223\ mAh \quad (6)$$

Therefore, on average, the molar ratio is about 223/5.5 ~ 40 Li:1 Gr, and does not go below 34:1 for the highest loading 3.6 mAh/cm^2 graphite. This is extreme excess; the lithium thickness was selected for ease of handling and supplier availability. We believe the protocol would work with much less Li.

Next, we conservatively estimate the capacity of irreversible Li formed at the Li metal electrode throughout the SOC-sweep protocol, assuming: 15 cycles, an average of 40% graphite capacity passed per cycle (~2 mAh), and 40% irreversibility for the plating/stripping of Li metal (should be higher due to the low ~0.6 mA/cm^2 plating current density on Li metal, see Manuscript Ref. 12 Fig. 1b, CCE electrolyte)

(15 cycles) · (2 mAh/cycle) · (0.4 irreversibility) = 12 mAh irreversible Li per cell

which gives the molar ratio of about 2.2 Li_{irrev}:1 Gr compared with the average 40 Li:Gr ratio in this work. Thus, we expect the quantity change to not influence results and expect much lower thicknesses of Li metal, on the order 0.2 mm instead of 0.75 mm, to provide sufficient lithium for these experiments.

Supplementary note 5 | Discussion of ambient temperature vs. fast-charging internal cell temperature

In the authors' previous thermal analysis of single-layer pouch cells using a similar Gr-NMC cell at rates of 1C-9C, the maximum computed temperature rise from 30ºC was 5ºC [Ref 9 Fig. 7a-b]. In the coin cells of this work, the high thermal mass and thermal conductivity of the stainless steel spacers, case and spring relative to the active material make us believe that the experimental temperature rise would be even lower. According to our Table 1 analysis, a ~3ºC increase in temperature from ambient would only change the plating onset by 2% SOC, giving us confidence that the conclusions of the study would still hold even if the data would shift slightly if measured temperatures were a few degrees higher than ambient.

Supplementary note 6 | Deciding on method for Graphite SOC shift calculation

Calculating the graphite SOC shift (ΔX), limited data points collected during 1C charging made it difficult to use dV/dQ peak positions, which are broader at the 1C charging rate, with the precision required for the analysis. Instead, we selected the x-position where the quantity Q_0 dV/dQ equals 1.0 V as the feature to monitor SOC shifting (Supplementary Fig. 27), because it occurs in the low-voltage regime of interest and precisely reports the change to ~1 µAh (Supplementary Fig. 28, Left). The value of 1.0 was selected arbitrarily and visual inspection of Supplementary Fig. 27, bottom, suggests any value between 0.8-1.2 V would give identical results. Supplementary Fig. 28 shows that significant SOC shift occurs from 1C cycling alone during the first ~30 1C cycles, and that the 1C cycle immediately following fast charging often has a value uniquely higher than cycles 2-5 after fast charging. The $(X_5 - X_3)$ correction subtracts any SOC shift anticipated from nominal cell formation or aging processes that occur in 2 1C cycles from the change observed over the 2 fast charging cycles.

Supplementary note 7 | Uncertainty analysis for converting full-cell SOC to graphite lithiation

$$x\ in\ Li_xC_6 = x_{initial} + SOC_{full-cell} \cdot \frac{C_{full-cell}}{C_{active\_graphite}} \quad (7)$$

Although Supplementary Fig. 37 analysis determined that $x_{initial}$ is 0.025 ± 0.001, this value is known to decrease throughout cycling because ΔX is consistently positive for each set of fast charging cycles (Supplementary Fig. 34). Integrating ΔX gives a total capacity shift throughout cycling, and dividing by $C_{active\_graphite}$ shows that the total decrease in initial lithiation is about 0.015. For the Li plating cycles that happen near the end of the protocol, we expect the average decrease in lithiation from the start to be about 0.01 ± 0.003, assumed to be a constant value to simplify analysis. Thus, $x_{initial}$ is presumed to be (0.025-0.01) = 0.015 ± 0.003. Combining the uncertainty contributions of $x_{initial}$ and $C_{active\_graphite}$ to $x\ in\ Li_xC_6$, the maximum uncertainty expected in the x-axis for Fig. 5b, at $SOC_{full-cell} = 0.9$ is:

$$\sigma_{x\ in\ LixC6} = \sqrt{\left(\frac{\partial x_{in\ LixC6}}{\partial x_{initial}}\right)^2 \sigma_{x_{initial}}^2 + \left(\frac{\partial x_{in\ LixC6}}{\partial C_{active_{gr}}}\right)^2 \sigma_{C_{active_{gr}}}^2} \quad (8)$$

$$= \sqrt{\sigma_{x_{initial}}^2 + \left(\frac{-0.9 \cdot 4.3}{5.24^2}\right)^2 \sigma_{C_{active_{gr}}}^2}$$

$$= \sqrt{0.003^2 + \left(\frac{-0.9 \cdot 4.3}{5.24^2}\right)^2 0.07^2} = \mathbf{0.010}$$

Supplementary note 8 | Calculating H_2 quantities from m/z = 2 ion current data

To calculate H_2 amounts from the online MST system, the following steps are taken and are based on previously developed knowledge of mass spectrometry application for titration experiments[7,8]. First, a value proportional to the H_2 mole fraction in the gas outlet, $\alpha \cdot y_{H2}$, where α is a proportionality factor, and is calculated from the ratio of m/z = 2 to m/z = 36 (Ar). We will denote this ion current signal ratio as $S_{2/36}$. Next, a linear baseline is applied to this data such that the first and final data points for each vial are 0, giving $S_{2/36,baselined}$. Then, the total system pressure P_{sys} for each data point is multiplied by this quantity to give a quantity proportional to the partial pressure of H_2. Finally, the ideal gas law is used to calculate a value proportional to the moles of H_2 in each sample, dn_{H2}, by knowing the lab temperature for each data point and the volume of the sample loop (2000 μL).

Thus, the moles of H_2 eluted in the i^{th} gas headspace sample is:

$$n_{H2,i} = \alpha \frac{V_{loop}}{R} \frac{S_{2/36,baselined,i}\ P_{sys,i}}{T_{sys,i}} \quad (9)$$

And the total moles of H_2 in a vial, related to the electrode titrated Li, is:

$$n_{H2,total} = \alpha \frac{V_{loop}}{R} \sum \frac{S_{2/36,baselined,i}\ P_{sys,i}}{T_{sys,i}} \quad (10)$$

Where the α proportionality factor is determined to be 1.96 x 10^{-4} from the calibration curve in Supplementary Fig. 24. This approach is different than our previous works, where α is explicitly estimated with other mass spectrometer gas calibration methods that require mixing the analyte gas (here H_2) with Ar at known pressures (concentrations) in-line.

Supplementary References

1. von Lüders, C. *et al.* Lithium plating in lithium-ion batteries investigated by voltage relaxation and in situ neutron diffraction. *J. Power Sources* **342**, 17–23 (2017).
2. Uhlmann, C., Illig, J., Ender, M., Schuster, R. & Ivers-Tiffée, E. In situ detection of lithium metal plating on graphite in experimental cells. *J. Power Sources* **279**, 428–438 (2015).
3. Chen, Y. *et al.* Operando video microscopy of Li plating and re-intercalation on graphite anodes during fast charging. *J. Mater. Chem. A* **9**, 23522–23536 (2021).
4. Konz, Z. M., McShane, E. J. & McCloskey, B. D. Detecting the onset of lithium plating and monitoring fast charging performace with voltage relaxation. *ACS Energy Lett.* **5**, 1750–1757 (2020).
5. Colclasure, A. M. *et al.* Requirements for Enabling Extreme Fast Charging of High Energy Density Li-Ion Cells while Avoiding Lithium Plating. *J. Electrochem. Soc.* **166**, A1412–A1424 (2019).
6. Finegan, D. P. *et al.* Spatial dynamics of lithiation and lithium plating during high-rate operation of graphite electrodes. *Energy Environ. Sci.* **13**, 2570–2584 (2020).
7. McShane, E. J. *et al.* Quantification of Inactive Lithium and Solid–Electrolyte Interphase Species on Graphite Electrodes after Fast Charging. *ACS Energy Lett.* **5**, 2045–2051 (2020).
8. Renfrew, S. E. & McCloskey, B. D. Residual Lithium Carbonate Predominantly Accounts for First Cycle CO_2 and CO Outgassing of Li-Stoichiometric and Li-Rich Layered Transition-Metal Oxides. *J. Am. Chem. Soc.* **139**, 17853–17860 (2017).
9. Colclasure, A. M. *et al.* Electrode scale and electrolyte transport effects on extreme fast charging of lithium-ion cells. *Electrochim. Acta* **337**, 135854 (2020).